bioRxiv preprint doi: https://doi.org/10.1101/2024.04.17.589812; this version posted April 26, 2024. The copyright holder for this preprint (which was not certified by peer review) is the author/funder, who has granted bioRxiv a license to display the preprint in perpetuity. It is made available under aCC-BY-NC-ND 4.0 International license.



# A Futile Cycle?

## Tissue Homeostatic Trans-Membrane Water Co-Transport:

## Kinetics, Thermodynamics, Metabolic Consequences.

**Charles S. Springer, Jr.[a-e] Martin M. Pike,[a,c,e] Thomas M. Barbara[a]**

**[a]Advanced Imaging Research Center, [b] Department of Chemical Physiology and Biochemistry, [c]Department of Biomedical Engineering, [d]Brenden-Colson Center for Pancreatic Care, [e]Knight Cancer Institute, Oregon Health & Science University; Portland, Oregon**

**Corresponding author:** C. S. Springer; springer@ohsu.edu
Advanced Imaging Research Center, L452
Oregon Health and Science University
3181 S. W. Sam Jackson Park Road
Portland, Oregon 97239

bioRxiv preprint doi: https://doi.org/10.1101/2024.04.17.589812; this version posted April 26, 2024. The copyright holder for this preprint (which was not certified by peer review) is the author/funder, who has granted bioRxiv a license to display the preprint in perpetuity. It is made available under aCC-BY-NC-ND 4.0 International license.



**ABSTRACT:**

The phenomenon of active trans-membrane water cycling (AWC) has emerged in little over a decade. Here, we consider $H_2O$ transport across cell membranes from the origins of its study. Historically, trans-membrane water transport processes were classified into: A) compensating bidirectional fluxes ("*exchange*"), and B) unidirectional flux ("*net flow*") categories. Recent literature molecular structure determinations and molecular dynamic (MD) simulations indicate probably all the many different hydrophilic substrate membrane co-transporters have membrane-spanning hydrophilic pathways and co-transport water along with their substrates, and that they individually catalyze category A and/or B water flux processes, although usually not simultaneously. The AWC name signifies that, integrated over the all the cell's co-transporters, the rate of *homeostatic*, bidirectional trans-cytolemmal water exchange (category A) is synchronized with the metabolic rate of the crucial $Na^+$,$K^+$-ATPase (NKA) enzyme. A literature survey indicates the stoichiometric (category B) water/substrate ratios of individual co-transporters are often very large. The MD simulations also suggest how different co-transporter reactions can be *kinetically* coupled molecularly.

Is this ($Na^+$,$K^+$-ATPase rate-synchronized) cycling futile, or is it consequential? Conservatively representative literature metabolomic and proteinomic results enable comprehensive free energy analyses of the many transport reactions with known water stoichiometries. Free energy calculations, using literature intracellular pressure ($P_i$) values reveals there is an *outward* trans-membrane $H_2O$ barochemical gradient of magnitude comparable to that of the well-known *inward* $Na^+$ electrochemical gradient. For most co-influxers, these gradients are finely balanced to maintain intracellular metabolite concentration values near their consuming enzyme Michaelis constants. The thermodynamic analyses include glucose, glutamate$^-$, gamma-aminobutyric acid (GABA), and lactate$^-$ transporters. 2%-4% $P_i$ alterations can lead to disastrous concentration levels. For the neurotransmitters glutamate$^-$ and GABA, very small astrocytic $P_i$ changes can allow/disallow synaptic transmission. Unlike the $Na^+$ and $K^+$ electrochemical steady-states, the $H_2O$ barochemical *steady-state* is in (or near) chemical *equilibrium*. The analyses show why the presence of aquaporins (AQPs) does not dissipate the trans-membrane pressure gradient. A feedback loop inherent in the opposing $Na^+$ electrochemical and $H_2O$ barochemical gradients regulates AQP-catalyzed water flux as an integral AWC aspect. These results also require a re-consideration of the underlying nature of $P_i$. Active trans-membrane water cycling is not futile, but is inherent to the cell's "NKA system" - a new, fundamental aspect of biology.

**SYNOPSIS:**

*Via* intracellular pressure, membrane co-transported water influences thermodynamic control of cell metabolite maintenance.

bioRxiv preprint doi: https://doi.org/10.1101/2024.04.17.589812; this version posted April 26, 2024. The copyright holder for this preprint (which was not certified by peer review) is the author/funder, who has granted bioRxiv a license to display the preprint in perpetuity. It is made available under aCC-BY-NC-ND 4.0 International license.



## INTRODUCTION:

One of the essential aspects of water in living tissue is its intra- extracellular compartmentalization. The kinetics of cellular, homeostatic trans-membrane water transport provides the basis of a new non-invasive, high-resolution MRI approach; metabolic activity diffusion imaging, MADI (1-3). It is providing novel views of cancer (4) and brain function (5) metabolism. Here, we inquire into kinetic, thermodynamic, and metabolic consequences of water co-transport phenomena in general.

**Distinct Trans-membrane Water Transport Processes:** Category B *unidirectional* "flux" processes driven by trans-membrane osmotic gradients have been extensively investigated (6,7). These are characterized by cell volume (V) changes [cell swelling/shrinking; edema; tissue hypertrophy]. Their kinetics are quantified with the "osmotic" [flux, flow] water permeability coefficient, $P_f$.

However, the earliest studies of which we are aware also detected category A *bidirectional* trans-membrane water "exchange" (8,9). In such processes, there is no V change – the systems are *homeostatic*. The kinetics are quantified with the "diffusional" water permeability coefficient, $P_d$. Initial studies employed isotopic labeling ($^2HO^1H$), requiring very rapid, careful solution mixing – to perturb the system from isotopic equilibrium. As tracer methods, such approaches yield the $P_d \bullet a_e$ product: $a_e = \rho\langle A\rangle$, where $\rho$ is the cell [number] density [cells/volume(tissue)] and $\langle A\rangle$ is the tissue-averaged cell surface area (1). [In the older literature, $a_e$ is given as S, the *total* cell surface area per tissue ["ensemble"] volume.] $P_d$ can be determined if $a_e$ can be estimated. Early $P_d$ values were compiled (10). We (11) and others showed that, at steady-state, $P_d$ confounds V and A with the homeostatic cellular water efflux rate constant, $k_{io}$, $P_d = (V/A)k_{io}$. It is $k_{io}$ that is a true measure of permeation probability (1). A nuclear magnetic resonance (NMR) approach was introduced in 1972 (12), which we later termed the "shutter-speed" (SS-NMR) method (13). Major SS-NMR advantages are it: **1.)** yields $k_{io}$ un-confounded, and separated from $(1 + ((\rho \bullet V - 1)/f_W))$: $f_W$ is the tissue water volume fraction (1,14); **2.)** does not require rapid solution mixing; and **3.)** could, in principle, quantify the category B flux and category A exchange processes simultaneously. An extracellular paramagnetic agent labels extracellular $^1H_2O$ magnetization, not extracellular water molecules (15), and non-invasive radio frequency electromagnetic pulses perturb the system magnetization from equilibrium. A compilation of early SS-NMR results was reported in (16). (Acronyms and symbols are listed in the **Appendix A1**).

**Molecular Aspects of Trans-membrane Water Transport:** Over the years, many membrane-bound macromolecules have been found to transport water between intra- and extracellular spaces. In 1988, Agre and co-workers reported the selective water transport protein aquaporin (AQP) family (17). The impressive array of different AQP variants now known has been reviewed (6). During the 1990's and 2000's, many other proteins were found to co-transport water molecules, along with the metabolic substrates for which they are named (reviewed in (18,19)). **Figure 1** shows AQP and

bioRxiv preprint doi: https://doi.org/10.1101/2024.04.17.589812; this version posted April 26, 2024. The copyright holder for this preprint (which was not certified by peer review) is the author/funder, who has granted bioRxiv a license to display the preprint in perpetuity. It is made available under aCC-BY-NC-ND 4.0 International license.



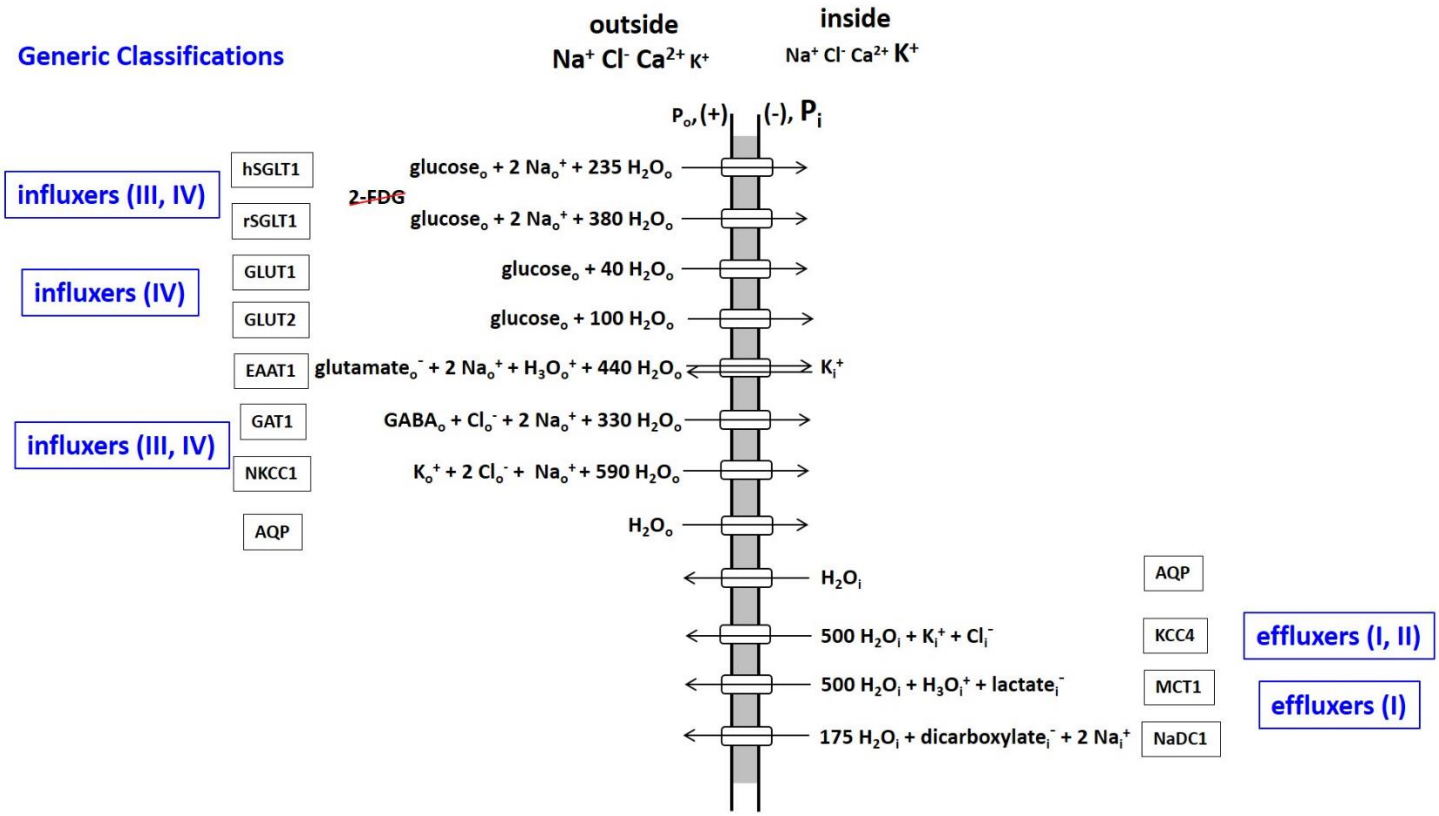


**Figure 1. An Inventory of water transporting membrane proteins.** The water stoichiometric values are taken from (19), and should be thought of as means of shot-to-shot variations (see text).

bioRxiv preprint doi: https://doi.org/10.1101/2024.04.17.589812; this version posted April 26, 2024. The copyright holder for this preprint (which was not certified by peer review) is the author/funder, who has granted bioRxiv a license to display the preprint in perpetuity. It is made available under aCC-BY-NC-ND 4.0 International license.



the ten water co-transporters detailed by Zeuthen (19). Each of their reactions is reversible, but here they are classified by their tendencies for influx or efflux under normal cellular conditions. These proteins all catalyze crucial processes, and are profitably considered as enzymes.

There are two glucose influx families: those co-transporting $Na^+$ (SGLT), and those that do not (GLUT). (Interestingly, though both families transport glucose, it has been recently noted (20) the SGLT family does not transport 2-deoxy-2-$^{18}$F-fluoro-D-glucose (2-FDG), the $^{18}$FDG-PET (positron emission tomography) glucose tracer. This can present interpretative problems.) The excitatory amino acid transporter (EAAT1) and the GABA transporter (GAT1) facilitate uptake of the principal excitatory and inhibitory neurotransmitters, glutamate$^-$ and GABA [the gamma-aminobutyric acid zwitterion], respectively. (In the Fig. 1 EAAT1 influx reaction, note the $H_3O^+$ co-influx, and the $K^+$ counter-*efflux* components (21).) The $Na^+$,$K^+$,2$Cl^-$ co-transporter (NKCC1) facilitates $K^+$ and $Cl^-$ influx (22).

The $K^+$,$Cl^-$ co-transporter (KCC4) provides an important pathway for $K^+$ and $Cl^-$ efflux (22). The monocarboxylic acid transporter (MCT1) extrudes the lactate$^-$ produced by cytoplasmic glycolytic-type metabolisms ($HCO_3^-$ is the analogous product of mitochondrial oxidative phosphorylation (23).

One is struck by the large water stoichiometries in most co-transporter cases. These values should be considered averages. Surely, they fluctuate stochastically (shot-to-shot) with each enzyme cycle (see below). Also, they likely vary with the cellular environment and biological condition. It is important to realize the Fig. 1 stoichiometries were determined in model systems *in vitro*, and by inducing net category B unidirectional fluxes (19). Homeostatic exchange was not studied in this regard.

In 1989, Ye and Verkman presented an elaborate optical method to measure $P_f$ and $P_d$ for *simultaneous* water efflux from and exchange in liposomes and in (adenosine tri-phosphate) ATP-free erythrocyte ghosts (24). Two very important results from that study are the following. First, a given water transporter can be involved in both category B flux and category A exchange processes, but not necessarily in the same proportions. Using $HgCl_2$ to inhibit AQP, the authors found while AQP contributes 90% of ghost water efflux, it accounts for only 45% of ghost exchange flux. Second, though $P_f$ for ghost efflux is numerically four times larger than $P_d$ for ghost exchange (in the same units), the time-course for water efflux is 50 times longer. The exchange process is much, much faster. A confusing aspect is that $P_f$ and $P_d$ are always reported with the same dimensions (length/time). However, the two permeability coefficients are defined by rate laws of very different natures ((7); (10), pp. 44 ff), and are not at all the same. The $P_f$ quantity characterizes transporter efficiency only in the presence of an osmotic gradient, and with the system perturbed from the steady-state. It gives no information on $P_d$.

**Active Trans-Membrane Water Cycling (AWC):** During most *in vitro* and *in vivo* studies, the tissue is in homeostasis: there is no substantial cell swelling or shrinking. Only category A trans-membrane water bidirectional *exchange* obtains.

bioRxiv preprint doi: https://doi.org/10.1101/2024.04.17.589812; this version posted April 26, 2024. The copyright holder for this preprint (which was not certified by peer review) is the author/funder, who has granted bioRxiv a license to display the preprint in perpetuity. It is made available under aCC-BY-NC-ND 4.0 International license.



Evidence mounts for a homeostatic, metabolic AWC process in cells (reviewed (1,2,15,25)). This is a very fast water molecule exchange, the kinetics of which are driven by, and synchronized to, those of the rate-limiting plasma membrane $Na^+$,$K^+$-ATPase (NKA) "sodium pump." The AWC phenomenon was first detected using water proton ($^1H_2O$) SS-NMR in 2011 (26). **Figure 2** is a cartoon illustrating the AWC process. For each NKA cycle, one intracellular $ATP_i$ molecule is hydrolyzed, three intracellular $Na_i^+$ ions expelled, and two extracellular $K_o^+$ ions imported. (First and second approximations of Fig 2 have appeared (2,15).) However, generic transporters II and III, respectively, allow $K^+$ to re-exit and $Na^+$ to re-enter exit the cell. Thus, NKA cycles extremely rapidly: depending on NKA expression, there can be $10^{10}$ ($Na^+$ + $K^+$) ions(cycled)/s/cell (15). These actions maintain the crucial trans-membrane ion concentration gradients, $[Na_o^+] > [Na_i^+]$, $[K_o^+] < [K_i^+]$; and the membrane electrical potential (in more negative than out, Figs. 1,2). Explicit examples of II and III are KCC4 and SGLT, respectively. The NKA substrates intracellular ATP and $Na^+$ and extracellular $K^+$ ($ATP_i$, $Na_i^+$, $K_o^+$, respectively) are rendered in red in Fig. 2, as is the natural product ouabain, a specific extracellular NKA inhibitor ($ouabain_o$).

Generic water co-transporters I and IV represent *secondary*, *active* obligate water symporters for water to exit and enter cells, respectively. Most of the Fig. 1 enzymes fit into this classification: they share substrates ($Na_o^+$ and/or $K_i^+$) with NKA, a *primary*, *active* transporter (hydrolyzes ATP directly). The first-order, unidirectional rate constants $k_{io}$ and $k_{oi}$ are those for *cellular*, *homeostatic* water efflux and influx, respectively. In the differential first-order chemical trans-membrane water transport rate law, $k_{io}$ can be expressed as the sum of energetically active, $k_{io}(a)$ and passive, $k_{io}(p)$, contributions that are further elaborated in **Equations (1)**, where: x is the overall, cellular AWC water

$$k_{io} = k_{io}(a) + k_{io}(p) = \left(\frac{x}{[H_2O_i]V}\right) {}^cMR_{NKA} + \left(\frac{A}{V}\right) P_W(p) \qquad (1)$$

stoichiometric coefficient ($H_2O$ molecules(cycled)/NKA(cycle)/s/cell), $[H_2O_i]$ the intracellular water concentration, ${}^cMR_{NKA}$ the cellular NKA metabolic rate (ATP(molecules hydrolyzed by NKA)/s/cell), and $P_W(p)$ the non-metabolic, passive *diffusive* water membrane permeability coefficient $P_d(p)$ (1,2,15). The influx rate constant, $k_{oi}$, is ρ-dependent, and also has active and passive components that need not be in the same proportions as for $k_{io}$. In healthy, living tissue, $k_{io}(p)$ and $k_{oi}(p)$ seem negligible (2). There can be $10^{12}$ ($H_2O$ molecules actively cycled)/s/cell (15). The value of x may be of magnitude $10^6$ (2).

The sodium pump is perhaps biology's most vital enzyme: it is found in all mammalian cells, and it's role in the evolution of life is thought crucial (27). Since NKA homeostatic activity has never before been accessible *in vivo*, medical MR imaging (MRI) applications of MADI are very promising (1,2,4,5). The water proton MR signal ($^1H_2O$) is by far the largest from tissue (28). The AWC-based MADI approach has been deemed "a new paradigm" (3).

bioRxiv preprint doi: https://doi.org/10.1101/2024.04.17.589812; this version posted April 26, 2024. The copyright holder for this preprint (which was not certified by peer review) is the author/funder, who has granted bioRxiv a license to display the preprint in perpetuity. It is made available under aCC-BY-NC-ND 4.0 International license.



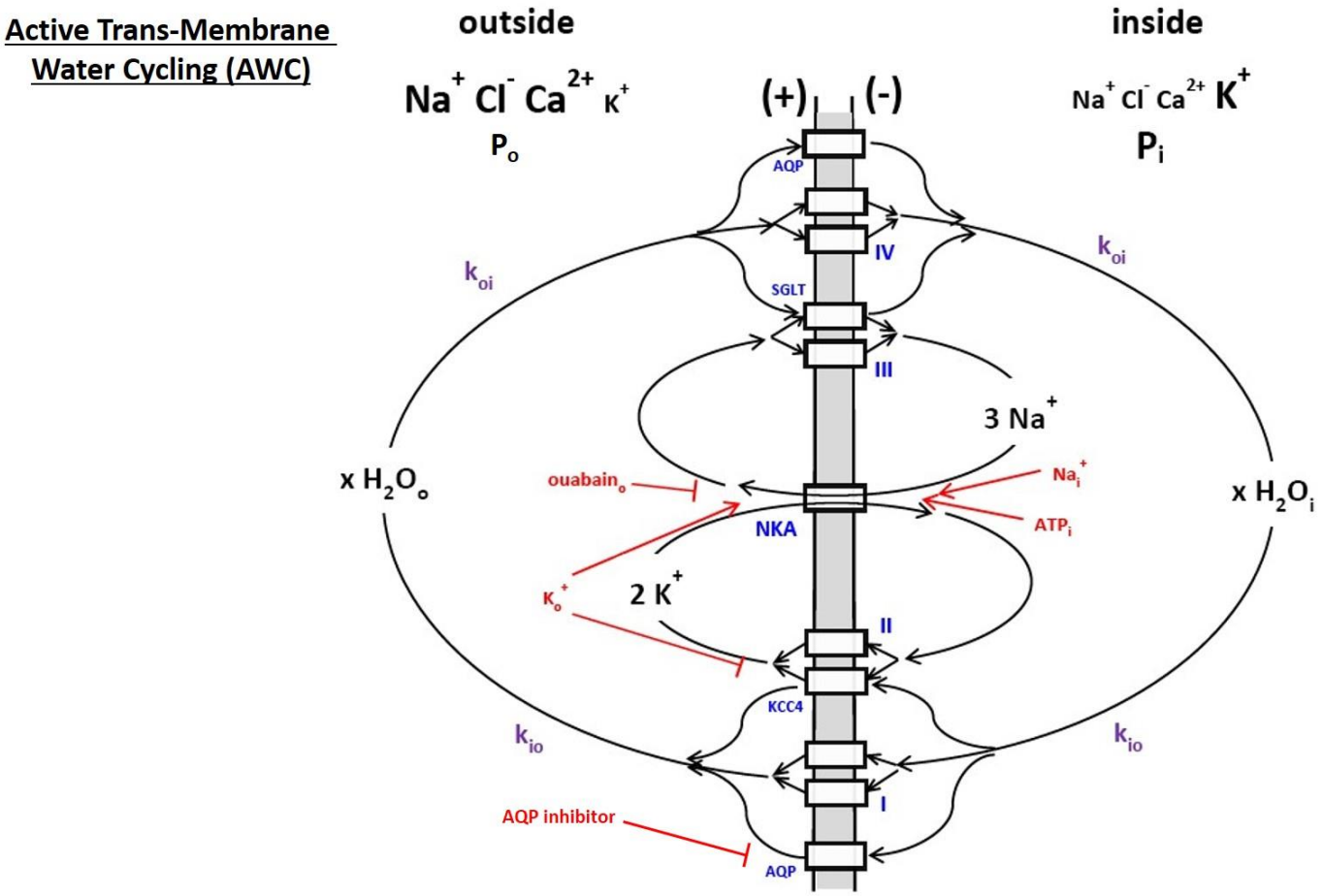


**Figure 2. A cartoon of active trans-membrane water cycling (AWC).** The rate constant for steady-state cellular water efflux is $k_{io}$; that for steady-state cellular water influx is $k_{oi}$. The $Na^+$,$K^+$-ATPase enzyme is indicated as NKA, while AQP, KCC4, and SGLT are defined in Figure 1. The actions of NKA substrates intracellular $Na^+$ and ATP ($Na_i^+$ and $ATP_i$) and extracellular $K^+$ ($K_o^+$) are indicated in red, as are the NKA inhibitor extracellular ouabain ($ouabain_o$) and an extracellular AQP inhibitor. Generic transporters I, II, III, and IV are exemplified in Figure 1: the actions of AQP, KCC4, and SGLT are shown here as specific examples. The quantity x is the AWC water stoichiometry integrated over the entire cell. Thus, for example, ${}^cMR_{H2O}$(influx) = ${}^cMR_{H2O}$(efflux) = $x{}^cMR_{NKA}$ = $x({}^cMR_{Na+}(\text{influx}))/3$ = $x({}^cMR_{K+}(\text{efflux}))/2$, where ${}^cMR$ represents a cellular metabolic rate. First and second approximations of this cartoon have appeared in (15) and (2), respectively.

bioRxiv preprint doi: https://doi.org/10.1101/2024.04.17.589812; this version posted April 26, 2024. The copyright holder for this preprint (which was not certified by peer review) is the author/funder, who has granted bioRxiv a license to display the preprint in perpetuity. It is made available under aCC-BY-NC-ND 4.0 International license.



Water-selective AQP transporters can also be involved in AWC as long there is a thermodynamic driving force for water flux (our calculations suggest their role in cellular homeostasis, see Discussion). AQP molecules themselves comprise simple, *passive* channels (29,30).

The existence of AWC has been demonstrated by many different, deliberate manipulations of NKA kinetics with, for example, $ATP_i$, $K_o^+$ and $ouabain_o$ concentration alterations (Fig. 2, red), while monitoring $k_{io}$. More than 20 independent studies, of a range of tissues, have been itemized (2,25). AWC can be mapped *in vivo* with non-invasive MADI, which estimates $k_{io}$, V, and ρ separately (1,2). In awake, resting human brain gray matter [GM], MADI mapping of the cellular water *flux* $[H_2O_i]k_{io}V = {}^cMR_{AWC}$, an $x^cMR_{NKA}$ estimate, correlates very well with the tissue metabolic rate of glucose consumption, $^tMR_{glu}$ (glucose(consumed)/s/unit volume(tissue)) determined from quantitative $^{18}$FDG-PET (2). This is expected: overall ATP production ($MR_{ATP}$) and consumption remain balanced in the resting brain. The white matter [WM] $^cMR_{AWC}/^tMR_{glu}$ ratio is larger than the GM $^cMR_{AWC}/^tMR_{glu}$ slope (2), likely indicating a more oxidative metabolic mechanism.

The most efficient $MR_{ATP}$ comes from mitochondrial oxidative phosphorylation (Fig. 2 of ref (15)), and $MR_{AWC}$ should be even more sensitive to this. Indeed, *in vitro* model brain tissue studies indicate $k_{io}V$ correlates strongly with mitochondrial $MR_{O2}$(consumption) (31). This is shown in **Figure 3** in the context of $MR_{NKA}$ stimulation *via* $[K_o^+]$ titration (Fig. 2). The vertical axis measures the population-averaged $\langle k_{io}\rangle_n$ for organotypic, cultured [spiking] rat somatosensory cortex superfused with a paramagnetic agent. This SS-NMR study also allowed the estimation that $\langle V\rangle_n$ was rather constant during the titration (Fig. 3D of ref. (31)): thus $\langle k_{io}\rangle_n$ was proportional to $\langle k_{io}V\rangle_n = \langle {}^cMR_{AWC}\rangle_n$. The horizontal axis measures $\langle {}^tMR_{O2}\rangle_n$, directly determined in completely independent $[K_o^+]$ titrations of isolated rat brain synaptosome suspensions. It is the $[K_o^+]$ titrations that allow this correlation: these are shown as outer ordinate and abscissa scales. They are non-linearly (Michaelis-Menten) related to the inner $\langle k_{io}\rangle_n$ and $\langle {}^tMR_{O2}\rangle_n$ scales, which are linear. The correlation is excellent over most of the range. (It is interesting $O_2$ consumption continues in the synaptosome suspensions even when $[K_o^+]$ is zero. This is not the case for $k_{io}$ in the SS-NMR study of cultured cortex preparations.) The quantity $k_{io}V$ is probably best thought of as a high-resolution *in vivo* measure of mitochondrial function.

In Figure 2, AWC participation of Fig. 1 enzymes is exemplified by SGLT (both a type III and a type IV transporter) and by KCC4 (a type II and type I enzyme). These transporters share substrates with NKA; $Na_o^+$ for SGLT and $K_i^+$ for KCC4. The SGLT and KCC4 reactions are thereby coupled with the NKA reaction. As individual proteins, I and IV respectively are catalyzing *unidirectional* water effluxes and influxes. Working in concert with other transporters, and orchestrated

bioRxiv preprint doi: https://doi.org/10.1101/2024.04.17.589812; this version posted April 26, 2024. The copyright holder for this preprint (which was not certified by peer review) is the author/funder, who has granted bioRxiv a license to display the preprint in perpetuity. It is made available under aCC-BY-NC-ND 4.0 International license.



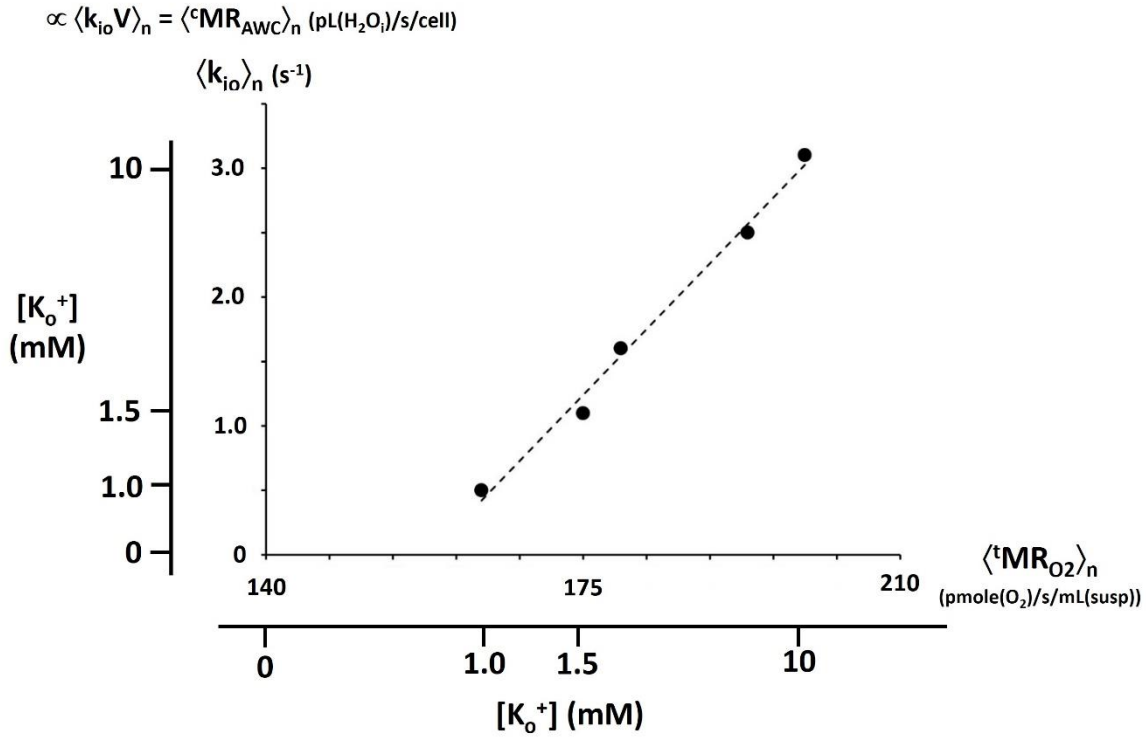


212

213

214 **Figure 3. A correlation of $k_{io}$ with $^{t}MR_{O2}$.** Independent [$K_o^+$] titrations of paramagnetic agent-superfused [SS-NMR]
215 studies of organotypic, cultured [spiking] rat somatosensory cortex [ordinate] and direct studies of isolated rat brain
216 synaptosome suspensions [abscissa] allow correlation of the population-averaged $\langle k_{io}\rangle_n$ and $\langle {}^{t}MR_{O2}\rangle_n$ quantities,
217 respectively. The outer [$K_o^+$] scales are non-linearly related to the linear, inner $\langle k_{io}\rangle_n$ and $\langle {}^{t}MR_{O2}\rangle_n$ scales due to their
218 Michaelis-Menten relationships. The correlation of $\langle k_{io}\rangle_n$ and $\langle {}^{t}MR_{O2}\rangle_n$ is very strong. The SS-NMR studies also indicate
219 the mean cell volume $\langle V\rangle_n$ is rather constant. Thus, $\langle k_{io}V\rangle_n$ = $\langle {}^{c}MR_{AWC}\rangle_n$ (pL($H_2O_i$)/s/cell) correlates with $\langle {}^{t}MR_{O2}\rangle_n$
220 (pmole($O_2$)/s/mL(suspension)). (This is a combination of Figures 3C and 3E of reference (31), where details are provided.
221 The points are synaptosome measurements: the dashed line is the Michaelis-Menten fitting ($K_m$ = 4.5 mM) of the cortical
222 culture measurements.)

223

224

bioRxiv preprint doi: https://doi.org/10.1101/2024.04.17.589812; this version posted April 26, 2024. The copyright holder for this preprint (which was not certified by peer review) is the author/funder, who has granted bioRxiv a license to display the preprint in perpetuity. It is made available under aCC-BY-NC-ND 4.0 International license.



by NKA activity however, they produce overall cellular homeostatic water *bidirectional* exchange. The cellular AWC fluxes are given in **Equation (2)**. This is a "systems" aspect of the cell. Though none of the individual process metabolic

$$\frac{{}^{c}MR_{Na+}(effl)}{3} = \frac{{}^{c}MR_{K+}(infl)}{2} = \frac{{}^{c}MR_{H2O}(effl)}{x} = {}^{c}MR_{NKA} = \frac{{}^{c}MR_{H2O}(infl)}{x} = \frac{{}^{c}MR_{K+}(effl)}{2} = \frac{{}^{c}MR_{Na+}(infl)}{3} \qquad (\mathbf{2})$$

rates ($^{c}$MR's) are equal to $^{c}MR_{NKA}$, they rise or fall with the latter. For example, $^{c}MR_{K+}(effl) = 2\,{}^{c}MR_{NKA}$ and $^{c}MR_{H2O}(effl) = x\,{}^{c}MR_{NKA} = [H_2O_i]k_{io}V$. Thus, $^{c}MR_{H2O}(effl) = {}^{c}MR_{H2O}(infl) = x\,{}^{c}MR_{NKA}$. NKA is the driver.

**Molecular Dynamics (MD):** *In silico* simulations of Fig. 1 transporter mechanisms using MD (29,30,32-37) can be very informative. This is particularly so for studies of an SGLT enzyme: the bacterial transporter vSGLT forms a hydrophilic membrane-spanning channel (32-36). Generally, the enzyme exhibits spasmodic (tens of ns) bursts, some featuring *net* water unidirectional influx and some featuring bidirectional water *exchange* (33-35). That is, a given transporter can indeed facilitate the net flux (category B) and the exchange (category A) processes at different times (32).

For a period after sodium ion release in the vSGLT sugar-bound state, water molecules pass inward and outward, past the galactose molecule (a glucose stereoisomer) in the channel, in almost equal, small numbers (~one molecule/ns) - homeostatic exchange. The sugar is bound to its site midway through the channel, while a $Na^+$ binding site is near the cytoplasmic mouth. In the ~100 ns after galactose is released, it proceeds through the channel into the cytoplasm, and pushes the channel-filling water molecules before it into the cell - net influx - in a quantity (33,35) generally consistent with the Fig. 1 SGLT water stoichiometries. Both such periods (exchange and net flux) are only transient (34). However, both seem triggered by $Na^+$ release.

Since the common role of the Fig. 1 enzymes is to facilitate passage of hydrophilic substrates across the hydrophobic bilayer membrane, it is likely they all have somewhat similar hydrophilic pathways. The structure of the NKCC1 transporter channel has been determined (38). We surmise there are many more water co-transporting membrane enzymes, possibly including $Na^+$,$K^+$-ATPase (NKA) itself, as yet unstudied for this aspect. The NKA channel structure has been elucidated (39). Transient exchange periods simulated for AQP-1 (37) are very similar to those for vSGLT (34). It is likely each of the Fig. 1 transporters can accomplish what AQPs accomplish, but in addition the conduct of specific metabolites across the membrane. Water molecules will find their ways through any open hydrophilic pathway ("pore").

The aforementioned vSGLT MD simulations also suggest possible molecular mechanisms for SGLT/NKA *kinetic* coupling. As stated, large tranches of net water molecule influx (category B) generally occur only upon galactose release from its site near the middle of the hydrophilic channel. But, the probability for this, and for exchange (category A), can

bioRxiv preprint doi: https://doi.org/10.1101/2024.04.17.589812; this version posted April 26, 2024. The copyright holder for this preprint (which was not certified by peer review) is the author/funder, who has granted bioRxiv a license to display the preprint in perpetuity. It is made available under aCC-BY-NC-ND 4.0 International license.



depend on whether a $Na^+$ ion is in a site: the $Na^+$ can block the sugar (and apparently *net* water) ingress into the cell (35,36). More often than not, $Na^+$ release occurs before sugar release (32). At least 80 ns after the $Na^+$ release (35,36), galactose release can occur – unless the $Na^+$ ion has re-bound or has been replaced by another $Na^+$ ion. While galactose is still present, the duty cycle of the $Na^+$ site remaining empty depends on the intracellular sodium concentration $[Na_i^+]$: this $Na^+$ can come from only inside the cell. With a normal ${}^cMR_{NKA}$, $[Na_i^+]$ is small (see below). However, $[Na_i^+]$ increases as ${}^cMR_{NKA}$ decreases (40). Thus, the probability of the $Na^+$ site being re-occupied within 80 ns increases as ${}^cMR_{NKA}$ decreases. As a consequence, the sugar-release frequency decreases as ${}^cMR_{NKA}$ decreases. In this way, $MR_{SGLT}$ and $MR_{NKA}$ are positively correlated kinetically. (This pair-wise SGLT/NKA consideration assumes all other Figs. 1,2 enzyme activities remain unchanged.) Irrespective of the details, the sharing of any substrate with NKA should facilitate kinetic coupling. The correlation mechanisms of other Fig. 1 water co-transporter activities with $MR_{NKA}$ must bear some general similarity to this. Pore openings and closings are metabolically controlled.

**A Futile Cycle?** When they were first realized, the Fig. 2 $Na^+$ and $K^+$ exchange processes may have been briefly viewed as "futile cycles." This term is used to characterize a set of coupled biochemical reactions that consume ATP with no apparent benefit (41). Obviously, it is generally thought biological evolution discards futile cycles as "energy wasting." However, it was quickly understood the trans-membrane ion concentration gradients enjoyed by $Na^+$ and $K^+$ serve to partially store chemical (Gibbs) free energy released by NKA-catalyzed ATP hydrolysis, $\Delta G_{ATP} = -59$ kJ/mole (42,43). As we will see below, $\Delta G_{Na}$(infl) is typically near – 14.5 kJ/mole, for $Na^+$ influx, and $\Delta G_K$(effl) near 0 kJ/mole, for $K^+$ efflux. Thus, though these cycles are *homeostatic*, they are not in *equilibrium*, but in *steady-state*. Energy is required to maintain them. Subsequently, the free energy thus stored in the $[Na^+]$ gradient is used to facilitate cellular uptake of many crucial molecules (Fig. 1), and these processes help complete the $Na^+$ cycle. The free energy in the $[K^+]$ gradient is small only because of the cell's membrane potential, which the homeostatic $K^+$ efflux largely produces and maintains (see below).

The "pump and leak mechanism" term used for water (19,27) implies waste. However, a question naturally arises. Might the existence of active trans-membrane water cycling (Fig. 2) reveal an analogous metabolic energy storage function? Is AWC an actual example of a futile cycle, or does it have some evolutionary advantage?

bioRxiv preprint doi: https://doi.org/10.1101/2024.04.17.589812; this version posted April 26, 2024. The copyright holder for this preprint (which was not certified by peer review) is the author/funder, who has granted bioRxiv a license to display the preprint in perpetuity. It is made available under aCC-BY-NC-ND 4.0 International license.



## THEORY:

**Reaction Free Energy Changes (ΔG):** The issue of AWC futility is a chemical thermodynamic question. Thus, we must consider ΔG for each permeant as it crosses the membrane, for example, into the cell; $\Delta G_{per}(infl)$, for *permeant* (per) influx (infl). For transport reactions (as in Fig. 1), the standard free energy change ($\Delta G^0$) is zero. There are potential chemogenic, electrogenic, and barogenic ΔG contributions. These are, respectively, the three terms on the right-hand-sides of **Equations (3)**; where i and o are, respectively, the inside and outside compartmental indices, [per] is

$$\Delta G_{per}\,(infl) = RTln\left\{\frac{[per_i]}{[per_o]}\right\} + Z_{per}FE_{m,oi} + RTln\left\{\frac{P_i}{P_o}\right\} = 2.58ln\left\{\frac{[per_i]}{[per_o]}\right\} + 0.0965Z_{per}E_{m,oi} + 2.58ln\left\{\frac{P_i}{P_o}\right\}\ \left(\frac{kJ}{mole}\right) \quad (3)$$

the compartmental permeant concentration, $Z_{per}$ the (signed) permeant particle electrical charge, F is the Faraday constant (0.0965 kJ/(mV•mole) at physiological temperature, 310 K), $E_{m,oi}$ is the (signed) trans-membrane electrical potential (in minus out) in mV, $P_i/P_o$ is the intracellular/extracellular hydraulic pressure ratio (Figs. 1,2) ((44), p. 35), and RT = 2.58 kJ/mole at 310 K. For $H_2O$ as permeant, $Z_{H2O} = 0$, and the second term makes no contribution.

Equations (3) can be written alternatively with permeant *chemical potential* changes; $\Delta\mu_{per}$, where $\mu_{per} \equiv (\partial G/\partial n_{per})_{T,P,n(\neq per)}$ ((44), p. 20). However, the ΔG notation is more inclusive, and more common in this field (42,43).

To obtain the free energy change for any Fig. 1 *reaction*, $\Delta G_{reac}(infl)$, one must sum over all permeants, **Equation (4)**; where $s_{per}$ is the permeant stoichiometric coefficient (Fig. 1). It is obvious from Eqs. (3,4) the chemogenic

$$\Delta G_{reac}\,(infl) = \sum_{per} s_{per}\left[2.58ln\left\{\frac{[per_i]}{[per_o]}\right\} + 0.0965Z_{per}E_{m,oi} + 2.58ln\left\{\frac{P_i}{P_o}\right\}\right] \qquad \left(\frac{kJ}{mole}\right) \quad (4)$$

terms require realistic compartmental permeant concentrations. Strictly, thermodynamic activity (a = the concentration•activity coefficient product) values should be used. Below, and in **A2**, we justify the first-order approximation that solute and solvent activity coefficients are each unity.

**Concentration Scales:** In this paper, a concentration is indicated with square brackets, *e.g.*, [permeant]. Sometimes, the molarity scale, with unit M = moles(permeant)/L(compartment) (activity coefficient $y_{per}$ ((45), pp. 26,27)) is used. However, first-order evaluation of chemogenic terms in Eqs. (3) and (4) consider only the entropy of mixing. This requires concentration scales with mole ratio- or mole fraction (X)-like quality. Molality, with unit m = moles(permeant)/kg(water) (activity coefficient $\gamma_{per}$ ((45), pp. 26,27)), is one such scale. Biological aqueous solutions are sufficiently dilute in each solute that its m value is well-approximated by its M value; the *infinite dilution* assumption. The use of an entropy-centric concentration scale here is tantamount to assuming solution "ideality;" there are no specific solute/solute interactions. We will see below this is clearly not the case. The "volume molality" scale, $_v$m = moles(permeant)/L(solvent) ((44), p.37) will also be considered. (Using m or $_v$m concentration values is tantamount

bioRxiv preprint doi: https://doi.org/10.1101/2024.04.17.589812; this version posted April 26, 2024. The copyright holder for this preprint (which was not certified by peer review) is the author/funder, who has granted bioRxiv a license to display the preprint in perpetuity. It is made available under aCC-BY-NC-ND 4.0 International license.



to assuming the small molecule metabolites may sample the entire compartmental space or only aqueous spaces, respectively, (*i.e.*, the water-excluding macromolecules are more or less mobile or immobile (14).) Since all the different neutral and ionic solutes (thus, osmolytes plural) need be counted, we will further use the OsMolarity (unit, OsM), or Osmolality (unit, Osm) concentration scales.

Since we also consider the solvent water as a permeant (Fig. 1), we must express its concentration. For understanding water thermodynamic activity – its "*escaping tendency*" - the dimensionless X (or a related) scale is best ((44), p. 56; (45), p.27; (46)). Thus, for water, $X_{H2O}$ = (moles(water))/(moles(osmolytes + water)), activity coefficient $f_{H2O}$ ((45), pp. 26,27)), is used.

One will further see milli- scales: mOsM, mOsm, and mOsX.

## Chemogenic Contributions

**Tissue Osmolyte Compartmental Concentrations.** For *in vivo* conditions, accurate determination of biological compartmental solute concentrations is difficult, particularly for intracellular metabolites. Recent metabolomic and proteomic advances (for example, using calibrated liquid chromatography/mass spectrometry techniques) have given realistic accountings. From such a study of cultured murine kidney epithelial cells, 101 different intracellular small molecule metabolites, and their concentrations, have been itemized (47). We compile an inventory of intra- and extra-cellular solute concentrations from a number of related studies (47-62) in **Table 1**. The inorganic ion ($Na^+$, $K^+$, $H_3O^+$, $Ca^{2+}$, $Mg^{2+}$, $Cl^-$, $HCO_3^-$) concentrations are conventional. The units are mOsM (thus, mOsm for osmolytes). These should be considered representative of interstitial and intracellular compartment osmolytes. Of course, they are not the values for any actual cell. Concentrations surely differ from cell to cell, tissue to tissue, and in different biological conditions. Since we are calculating general thermodynamic trends, the Table 1 values suffice.

We see the intracellular RNA, lipid assembly, and DNA mOsM concentrations are tiny. Though these occupy considerable intracellular volume (see below), because of their very large macromolecular masses they make negligible osmolal contributions. Since there are fewer (but non-zero: see below) extracellular macromolecules, we ignore their osmolal contributions here.

Interestingly, we see the total osmolyte concentrations are ~0.3 OsM for the interstitial space and ~0.4 OsM for the intracellular space. It is widely assumed intracellular osmolarity is near 0.3 (52), and thus similar to that in the extracellular space. The implications of this trans-membrane osmolarity gradient are explored in the section on intracellular pressure ($P_i$) below.

bioRxiv preprint doi: https://doi.org/10.1101/2024.04.17.589812; this version posted April 26, 2024. The copyright holder for this preprint (which was not certified by peer review) is the author/funder, who has granted bioRxiv a license to display the preprint in perpetuity. It is made available under aCC-BY-NC-ND 4.0 International license.



339

340

| Table 1. Representative Osmolyte Concentrations (mOsM)[a-d] | | |
|---|---|---|
| | **interstitial** | **intracellular** |
| **$Na^+$** | 135.0 | 15.0 |
| **$K^+$** | 5.0 | 150.0 |
| **$H_3O^+$** | 0.00005 | 0.0001 |
| **$Ca^{2+}$** | 1.5 | 0.0001 [free]; 0.01 [total] |
| **$Mg^{2+}$** | 0.5 | 0.5 [free]; 10 [total] |
| **other cations** | 1.5 | 3.5 |
| **$Cl^-$** | 105.0 | 15.0 |
| **$HCO_3^-$** | 30.0 | 10.0 |
| **small molecule metabolite anions** | 3.0 | 135.0[a,b] |
| **protein anions** | 7.5[a] | 9.5[a,c,d] |
| **small molecule metabolites** | | 40.0[a,b] |
| **RNA** | | 0.5[d] |
| **lipids** | | 0.05[d] |
| **DNA** | | 0.000005[d] |
| **total osmolytes** | 289 | 379 |
| | | |
| **$H_2O$ mole fraction ($OsX_W$)** | 0.995 | 0.993 |
| | | |
| **$H_2O$ millimolarity (mM)** | 45,000[e] | 42,000[f] |
| **$f_W$** | $f_{W,o}$ = 45/55 = 0.82 | $f_{W,i}$ = 42/55 = 0.76 |
| **osmotic stoichiometry ($H_2O$/osmolyte)** | 45/0.289 = ~156 | 42/0.379 = ~111 |
| **References (47-62). [a]ref. (48), [b]ref. (47), [c]ref. (49), [d]ref. (50), [e]ref. (62), [f]ref. (51).** | | |

341

342

343

bioRxiv preprint doi: https://doi.org/10.1101/2024.04.17.589812; this version posted April 26, 2024. The copyright holder for this preprint (which was not certified by peer review) is the author/funder, who has granted bioRxiv a license to display the preprint in perpetuity. It is made available under aCC-BY-NC-ND 4.0 International license.



**Tissue Water Compartmental Concentrations.** Experimentally determining biological compartmental water contents is even harder than for solutes (2). For many years, it has been stated, usually anecdotally, that cell water content is 70% (v/v) [or (w/w), assuming unit density, d] (53). Vinnakota and Bassingthwaighte presented a comprehensive review and tabulation of rigorous, quantitative determinations of myocardial tissue compartmental densities, volumes, volume fractions, and mass fractions (51). These derive from direct *ex vivo* mass analyses and *in vivo* tracer studies, and yield the cell water content value 75 % (w/w). A more recent optical determination yields 85 % (v/v) for cultured mammalian cell controls (54).

If we use the 75 % value (51) and take d = 1.1 g/mL, we obtain $[H_2O_i]$ = 42 M; *i.e.*, 42 moles($H_2O$)/L(cell). This is the most parsimonious interpretation of the data, and includes water in the cytoplasm, mitochondria, and sarcoplasmic reticula. The magnitude is considerably reduced from the value for pure water, 55 M. The intracellular water volume fraction, $f_{W,i}$, estimated from this is 42/55 = 0.76 (Table 1). This is in good agreement with quantitative MRI *in vivo* measures (55). (Note: $f_W$ is different from $f_{H2O}$.) Rand states, without attribution, $[H_2O_i]$ = 54 M (56).

From tracer ($^{15}OH_2$) studies (reviewed in (51)) and NMR ($^1H_2O$) studies (reviewed in (2)), essentially all intracellular water is effectively "well-mixed," at homeostasis. There has been much consideration of "bound" water in tissue (reviewed in (25,57-59)). There is no doubt water near macromolecule and membrane surfaces is thermodynamically different from bulk water – it has at least lower entropy (see below) – but kinetically (tumbling- and diffusion-wise) it remains in very rapid communication with all the water in the cell. The fraction of water molecules in "buried" intra-macromolecular sites inside cells is miniscule. Though the latter have significant NMR consequences (reviewed in (25)), even these water molecules have labile access to the cytoplasm (60).

Because of its small volume fraction (typically, 0.2) the extracellular compartmental water content in parenchymal tissue has been even more difficult to determine. Vinnakota and Bassingthwaighte report myocardial *interstitial* water content 92 % (w/w) and d = 1.0 g/mL, but this has a significantly greater uncertainty (51) and seems excessively large. The water content of cartilage can be more directly determined, and this might be a good extracellular model: it is an essentially acellular matrix of collagen fibrils (61). Lu and Mow imply a cartilage water content value of 78 % to 85 % (61). Maroudas and co-workers carefully measured the value 81 % for unloaded human femoral head cartilage (62). Again assuming unit density, this yields $[H_2O_o]$ = 45 M, also significantly reduced from 55 M, though not as much as $[H_2O_i]$. The corresponding $f_{W,o}$ is 45/55 = 0.82 (Table 1).

In Table 1, we give intra- and extracellular "osmotic stoichiometry" values; the overall ratio of water molecules to osmolyte particles in the compartment. We see the intra- and extracellular values are near 100 and 150 water molecules per osmolyte, respectively. The fact that in Fig. 1 transporter osmotic stoichiometries for the reactants are either above or below these values is consistent with the water stoichiometry being principally determined by the hydrophilic channel volumes (35). The molecular action of any particular transporter has nothing to do with

bioRxiv preprint doi: https://doi.org/10.1101/2024.04.17.589812; this version posted April 26, 2024. The copyright holder for this preprint (which was not certified by peer review) is the author/funder, who has granted bioRxiv a license to display the preprint in perpetuity. It is made available under aCC-BY-NC-ND 4.0 International license.



the overall "osmotic stoichiometry." It is only the *net* water transported by all influxers and effluxers in the cell that must be zero for homeostasis. However, even if values of 100 or 150 did obtain, this would be irrelevant for the calculations below.

The large macromolecular volumes are the reason the 42 M intracellular $H_2O$ concentration (Table 1) used below is so much less than that of pure water (55 M). These large molecules exclude considerable water (Fig. 8 of (15)). Obviously, there are also water-displacing extracellular macromolecules: 45 M (Table 1) is also smaller than 55 M.

However, the molar concentration scale is useful mainly for molecular counting (1 mole = 6 x $10^{23}$ molecules). As justified above, we use the dimensionless mole fraction concentration scale for water ($X_{H2O}$). (This differs from the tissue compartmental water mole fractions ("populations") $p_i$ and $p_o$ (important in SS-NMR).) For most practical aqueous solutions, including those in biological compartments, however, $X_{H2O}$ is always very nearly unity. "In dilute solutions of electrolytes, the activities, and even the activity coefficients ($f_{H2O}$), of the *solvent* are little different from unity" ((63), p.12). Very important consequences of this are considered below.

One kg of water is (1000/18.0154) 55.508 moles $H_2O$. Dividing this by (55.508 + the sum of osmolyte concentrations) in each of the cytosolic and interstitial compartments yields corresponding water mole fractions $OsX_{H2O,i}$ = 0.993 and $OsX_{H2O,o}$ = 0.995 (Table 1). $OsX_{H2O,i}$ is only 0.2% smaller than $OsX_{H2O,o}$, and each value is nearly that for pure water. Given this situation, following Pitzer ((63), p.12), it is not unreasonable to assume equal activity coefficients ($f_{H2O,i} = f_{H2O,o} = 1$) and thus use these mole fraction values in the Eqs. (3) and (4) terms for water as permeant. Inserting $\{OsX_{H2O,i}/OsX_{H2O,o}\}$ = 0.998 yields $\Delta G_{H2O}$(infl) = **-** 0.00517 kJ/mole for the *chemogenic* contribution.

Therefore, unlike the other Table 1 species, water is almost (but not exactly) in trans-membrane chemical equilibrium. (In this paper, "*chemical*" equilibrium is defined as: $[per_i] = [per_o]$.) There is (only) ~5 J/mole favoring cellular water influx. Strictly, this chemogenic $\Delta G_{H2O}$(infl) value might be considered not significantly different from zero (chemical equilibrium). However, analyses of surrogate solutions in **A2** give water activity values: $a_{H2O,i}$ = 0.994 and $a_{H2O,o}$ = 0.995. These correspond to chemogenic $\Delta G_{H2O}$(infl) = **-** 0.003 kJ/mole. Henceforth, we will use – 3 J/mole. As we will see, this has no bearing on the important metabolic consequences detailed below. For co-transported water, the barogenic contribution will be much greater than the chemogenic term.

It is probably unreasonable that chemogenic $\Delta G_{H2O}$(infl) be positive. First-order osmotic considerations more strongly favor water influx. However, the first-order is inadequate, see below.

bioRxiv preprint doi: https://doi.org/10.1101/2024.04.17.589812; this version posted April 26, 2024. The copyright holder for this preprint (which was not certified by peer review) is the author/funder, who has granted bioRxiv a license to display the preprint in perpetuity. It is made available under aCC-BY-NC-ND 4.0 International license.



## Electrogenic Contributions

We make the common approximation that $K^+$ *efflux* permeabillity dominates over $Na^+$ and $Cl^-$ permeabilities (in the $P_f$ sense) in cellular homeostasis. Thus, we use a version of the Nernst **Equation (5)** ((44), p. 113) to calculate $E_{m,oi}$,

$$E_{m,oi} = -\left(\frac{RT}{FZ_{K+}}\right)\left\{ln\left(\frac{[K_i^+]}{[K_o^+]}\right)\right\} = \left(\frac{2.58}{0.0965}\right)\left\{ln\left(\frac{150}{5}\right)\right\} = -91\ mV \qquad (5)$$

where: RT = 2.58 kJ/mole and the Faraday constant F = 0.0965 kJ/mV•mole (both at 310 K) and insert the Table 1 $[K^+]$ values. Z must be the value for the potential-producing ion, $Z_{K+} = 1$. It is important to note the actual number of *excess* $K_o^+$ ions (and an equal number of uncompensated intracellular anions) is insufficient to significantly alter the Table 1 $[K^+]$ values. An excess of only 0.02 mM intracellular anionic charges (0.014% = ((100x0.02)/145); Table 1) produces $E_{m,oi} \approx$ - 100 mV for a small (1 fL) spherical cell ((53), p. 198.)

## Barogenic Contributions

Intracellular pressure ($P_i$) can be counteracted with an externally applied (macroscopically uniform) mechanical pressure, in principle ((44), p.32), and elegantly transduced into an isotropic, hydraulic (mechanical) pressure with cellular insertion of a pressure-sensitive "osmotic" microelectrode (64,65). The trans-membrane pressure difference ($P_i - P_o$) force is oriented roughly vectorially radial to the cell surface. Experimentally, most mammalian cells have ($P_i$ - $P_o$) values under 0.1 atm (27). However, an osmotic microelectrode study of perfused *ex vivo* murine lens (featuring relatively simple lens cells) found ($P_i$ - $P_o$) values up to 0.5 atm (66). Most $P_o$ values are near 1 atm: even "high" tumor interstitial $P_o$ is only 1.02 atm. (67). For water, the standard state ($f_{H2O}$ truly 1) pressure, $P^0$, is 1.0 atm.

bioRxiv preprint doi: https://doi.org/10.1101/2024.04.17.589812; this version posted April 26, 2024. The copyright holder for this preprint (which was not certified by peer review) is the author/funder, who has granted bioRxiv a license to display the preprint in perpetuity. It is made available under aCC-BY-NC-ND 4.0 International license.



## RESULTS:

### Free Energy Calculations

***Permeant* Influx Free Energy Changes, Eq. (3).** In **Table 2**, we list many potential non-metabolite permeant (per) species, and calculate chemogenic, electrogenic, and barogenic $\Delta G$(infl) contributions (kJ/mole) for their influx. For these calculations, we use the Table 1 water $OsX_W$ and solute mOsm concentrations for the chemogenic terms. We calculate the barogenic contributions for $P_i/P_o$ ratios of 1.00 (blue) and 1.05 (red).

It is clear that, compared with those of the other permeants, the chemogenic and electrogenic contributions for individual $H_2O$ molecule transport are negligible. We see the slight chemogenic tendency for water molecule influx when $P_i = P_o$ is reversed when $P_i \geq 1.05\ P_o$. In fact, for $\Delta G_{H2O}$(infl) = - 0.003 kJ/mole, any $P_i > 1.001\ P_o$ would result in water efflux if there were no other considerations.

Let us consider two other potential permeants, $Na_o^+$ and $K_o^+$ as examples. The electrogenic terms for their *influxes* are identical, - 8.78 kJ/mole. Electrostatically, influx of each is favored. However, while the chemogenic $Na_o^+$ contribution (- 5.67 kJ/mole) also favors influx, the chemogenic $K_o^+$ term (8.78 kJ/mole) opposes influx. Thus, the *electrochemical* potential gradient for $Na_o^+$ influx is very favorable, – 14.5 kJ/mole (- 5.67 – 8.78), but zero for $K_o^+$ influx (or $K_i^+$ efflux) when $P_i = P_o$. The barogenic contributions for $Na_o^+$ and $K_o^+$ are identical, but this has very small effect for only $Na_o^+$. However, compared with $Na_o^+$, and indeed with all the other Table 2 permeants except $K_o^+$, the barogenic contribution for $H_2O$ is *proportionally* much greater than the chemo- and electrogenic terms. (For example, a $P_i$ of 1.05 atm causes a more than 40-fold increase in $\Delta G_{H2O}$, but only a 1% change in $\Delta G_{Na}$.) This has very important consequences.

**Transport *Reaction* Free Energy Changes, Eq. (4).** We use Eq. (4) to calculate the total $\Delta G_{transporter}$(infl) for each of the Fig. 1 transporter reactions - utilizing the stoichiometries seen there. The "metabolite" substrates (glucose, glutamate$^-$, GABA, and lactate$^-$) are omitted because we study below how their transport is affected by the thermodynamic contributions of the other "ancillary" (support) substrates.

Influx Reactions. Reactions that normally run in the *influx* direction (IV, III, or both, in Figs. 1,2) are presented in **Table 3a** ($E_{m,oi}$ is fixed at – 91 mV). Each is favorable (negative $\Delta G$) when $P_i = P_o$ (blue). However, they each become less favorable as $P_i/P_o$ increases, and all become unfavorable (positive $\Delta G$) when $P_i$ has reached 1.05 $P_o$ (red). This is due to $P_i$ opposition to water co-influx (the factors that are - 0.003 when $P_i = P_o$ become positive when $P_i$ exceeds 1.001 $P_o$). Because of the large water stoichiometries, the barogenic contribution can have a significant influence on secondary active water co-transporter thermodynamics. This is due to essentially only the water co-transport. For the other permeants, the blue/red values generally have very similar magnitudes.

bioRxiv preprint doi: https://doi.org/10.1101/2024.04.17.589812; this version posted April 26, 2024. The copyright holder for this preprint (which was not certified by peer review) is the author/funder, who has granted bioRxiv a license to display the preprint in perpetuity. It is made available under aCC-BY-NC-ND 4.0 International license.



**Table 2. Free Energy Change for Influx, Eq. (3).**

| potential permeant | $\Delta G_{per}$(infl) (kJ/mole) | | | |
|---|---|---|---|---|
| | chemogenic | electrogenic | barogenic | sum |
| | | | $P_i/P_o$ = 1.00 \|\| 1.05 | $P_i/P_o$ = 1.00 \|\| 1.05 |
| $H_2O_o$ | -0.003 | 0 | 0 \|\| 0.13 | -0.003 \|\| 0.13 |
| $Na_o^+$ | -5.67 | -8.78 | 0 \|\| 0.13 | -14.5 \|\| -14.3 |
| $K_o^+$ | 8.78 | -8.78 | 0 \|\| 0.13 | 0 \|\| 0.13 |
| $H_3O_o^+$ | 1.79 | -8.78 | 0 \|\| 0.13 | -6.99 \|\| -6.86 |
| $Ca_o^{2+}$ | -24.8 | -17.6 | 0 \|\| 0.13 | -42.4 \|\| -42.3 |
| $Cl_o^-$ | -5.02 | 8.76 | 0 \|\| 0.13 | 3.74 \|\| 3.87 |
| $HCO_{3,o}^-$ | -2.83 | 8.76 | 0 \|\| 0.13 | 5.93 \|\| 6.06 |

Concentrations in Table 1. $E_{m,oi}$ = -91 mV

bioRxiv preprint doi: https://doi.org/10.1101/2024.04.17.589812; this version posted April 26, 2024. The copyright holder for this preprint (which was not certified by peer review) is the author/funder, who has granted bioRxiv a license to display the preprint in perpetuity. It is made available under aCC-BY-NC-ND 4.0 International license.



463

| Table 3a. Transport Reaction Free Energy Changes, ΔG(infl) (kJ/mol); Eq. (4) ($P_i/P_o$ = 1.00 \|\| 1.05) | | | | | |
|---|---|---|---|---|---|
| influxer reactions [III, IV, or both, in Fig. 1) w/o metabolic substrates | | | | | |
| enzyme | substrates and free energies | | | | net |
| hSGLT1 | $glucose_o$ + | 2 $Na_o^+$ + | 235 $H_2O_o$ → | | |
| | | 2(-14.5 \|\| -14.3) | 235(-0.003 \|\| 0.13) | | |
| | | (-29 \|\| -28.6) + | (-0.71 \|\| 31) = | | (-29.7 \|\| 2.4) |
| rSGLT1 | $glucose_o$ + | 2 $Na_o^+$ + | 380 $H_2O_o$ → | | |
| | | 2(-14.5 \|\| -14.3) | 380(-0.003 \|\| 0.13) | | |
| | | (-29 \|\| -28.6) + | (-1.1 \|\| 49) = | | (-30 \|\| 20.4) |
| GLUT1 | $glucose_o$ + | | 40 $H_2O_o$ → | | |
| | | | 40(-0.003 \|\| 0.13) | | |
| | | | (-0.12 \|\| 5.2) = | | (-0.12 \|\| 5.2) |
| GLUT2 | $glucose_o$ + | | 100 $H_2O_o$ → | | |
| | | | 100(-0.003 \|\| 0.13) | | |
| | | | (-0.30 \|\| 13) = | | (-0.30 \|\| 13) |
| EAAT1 | $glutamate_o^-$ + | 2 $Na_o^+$ + | 440 $H_2O_o$ + | - $K_i^+$ + $H_3O_o^+$ → | |
| | | 2(-14.5 \|\| -14.3) | 440(-0.003 \|\| 0.13) | | |
| | | (-29 \|\| -26.8) + | (-1.3 \|\| 57) = | (0 \|\| -0.13) + (-6.99 \|\| -6.86) = | (-37 \|\| 23) |
| GAT1 | $GABA_o$ + | 2 $Na_o^+$ + | 330 $H_2O_o$ + | $Cl_o^-$ → | |
| | | 2(-14.5 \|\| -14.3) | 330(-0.003 \|\| 0.13) | | |
| | | (-29 \|\| -26.8) + | (-0.99 \|\| 43) = | (3.74 \|\| 3.87) = | (-26 \|\| 20) |
| NKCC1 | 2$Cl_o^-$ + | $Na_o^+$ + | 590 $H_2O_o$ + | $K_o^+$ → | |
| | 2(3.74 \|\| 3.87) | | 590(-0.003 \|\| 0.13) | | |
| | (7.48 \|\| 7.74) | (-14.5 \|\| -14.3) | (-1.77 \|\| 77) | (0 \|\| 0.13) | (-8.8 \|\| 71) |
| All stoichiometries from reference (19). $\Delta G_{pcr}$, from Table 2. $E_{m,oi}$ = -91 mV | | | | | |

464

465

466

bioRxiv preprint doi: https://doi.org/10.1101/2024.04.17.589812; this version posted April 26, 2024. The copyright holder for this preprint (which was not certified by peer review) is the author/funder, who has granted bioRxiv a license to display the preprint in perpetuity. It is made available under aCC-BY-NC-ND 4.0 International license.



**Table 3b, Transport Reaction Free Energy Changes, ΔG(effl) (kJ/mol), Efflux Version of Eq. (4) ($P_i/P_o$ = 1.00 || 1.05)**

**effluxer reactions (I, II, or both, in Fig. 1) w/o metabolic substrates**

| KCC4 | $K_i^+$ + | $Cl_i^-$ + | 500. $H_2O_i$ → | | net |
|---|---|---|---|---|---|
| | (0 \|\| -0.13) + | (-3.74 \|\| -3.87) + | 500(0.003 \|\| -0.13)<br>(1.5 \|\| -65) = | | (-2.2 \|\| -69) |
| **MCT1** | **lactate$_i^-$ +** | **$H_3O_i^+$ +** | **500 $H_2O_i$ →** | | |
| | | (6.99 \|\| 6.86) + | 500(0.003 \|\| -0.13)<br>(1.5 \|\| -65) = | | (8.5 \|\| -58) |
| **NaDC1** | **dicarboxylate$_i^{2-}$ +** | | **175 $H_2O_i$ +** | **2 $Na_i^+$ →** | |
| | | | 175(0.003 \|\| -0.13)<br>(0.53 \|\| -23) + | 2(14.5 \|\| 14.3)<br>(29 \|\| 29) = | (30 \|\| 6.0) |

All stoichiometries from reference (19). $-\Delta G_{per}$(infl) from Table 2. $E_{m,oi}$ = -91 mV

bioRxiv preprint doi: https://doi.org/10.1101/2024.04.17.589812; this version posted April 26, 2024. The copyright holder for this preprint (which was not certified by peer review) is the author/funder, who has granted bioRxiv a license to display the preprint in perpetuity. It is made available under aCC-BY-NC-ND 4.0 International license.



Glucose Uptake at Fixed [glucose$_i$]. For the rSGLT1 influx reaction as an example: $\Delta G$ = - 30 kJ/mole when $P_i = P_o$, but 20.4 kJ/mole when $P_i$ = 1.05 $P_o$. ($P_i$ = 1.03 $P_o$ is sufficient to make influx unfavorable.) To illustrate the consequences of this on glucose uptake, we fix the intracellular glucose concentration, [glc$_i$], at 2 µM. (The intracellular enzyme that phosphorylates glucose, hexokinase, has a glucose$_o$ $K_m$ value reported as 1.7 µM (20). A principle of central carbon (glucose-related) metabolism is that any intracellular metabolite steady-state concentration should be near the $K_m$ value of the enzyme that consumes it (47).) Thus, we write Eq. (4) explicitly for the $2Na^+$/glucose co-transporter **rSGLT1** influx free energy change, $\Delta G_{rSGLT1}(infl)$, in **Equation (6)**. The first term represents the glucose barochemical contribution

$$\Delta G_{rSGLT1}(infl) = \left[2.58ln\left\{\frac{2}{[glc_o]}\right\} + 2.58ln\left\{\frac{P_i}{P_o}\right\}\right] + 2\left[-5.67 - 8.78 + 2.58ln\left\{\frac{P_i}{P_o}\right\}\right] + 380\left[-0.003 + 2.58ln\left\{\frac{P_i}{P_o}\right\}\right] \quad (6)$$

with [glc$_i$] fixed at 2 µM. The second and third terms are due to, respectively, the $Na^+$ electro- and barochemical and the $H_2O$ barochemical potential gradients. The former favors influx, while the latter opposes it.

If we fix $P_i$ = 1.05 $P_o$, and neglect the water co-transport, $\Delta G$ becomes positive (*i.e.*, influx ceases) only when the extracellular glucose concentration [glc$_o$] decreases below 0.33 nM. On the other hand, if we keep $P_i$ = 1.05 $P_o$ but retain the water co-transport, the reaction becomes unfavorable when [glc$_o$] decreases below 2.4 mM – three orders of magnitude *greater than* [glc$_i$]. The large electrochemical $\Delta G_{Na+}$ favoring influx (- 28.6 kJ/mole) is counteracted by the even larger barochemical $\Delta G_{H2O}(infl)$ favoring efflux (49 kJ/mole). A number of significant consequences of this will be considered in the Discussion section.

To partially generalize these considerations, **Figure 4** shows a 3D plot of Eq. (6) for the rSGLT1 reaction. For this, the [$Na_o^+$] and [$Na_i^+$] values were fixed at those in Table 1, [glc$_i$] at 2 µM, and $E_{m,oi}$ at – 91 mV. The vertical axis plots the rSGLT1 influx reaction $\Delta G_{rSGLT1}(infl)$, while the (logarithmic) oblique axes increment [glc$_o$] and $P_i/P_o$. The free energy surface is colored green when influx is possible ($\Delta G_{rSGLT1}(infl) < 0$), and red when impossible ($\Delta G_{rSGLT1}(infl) > 0$). The intersection of the $\Delta G_{rSGLT1}(infl)$ surface with the horizontal $\Delta G_{rSGLT1}(infl) = 0$ plane defines the trajectory of the ($P_i/P_o$)-dependence of the minimum extracellular glucose concentration required for influx. While the exponential nature of the ($P_i/P_o$)-dependence is hardly noticeable, that of [glc$_o$] is very evident.

To make these effects clearer, **Figure 5** shows the 2D plot of the Fig. 4 $\Delta G_{rSGLT1}(infl) = 0$ plane. With $H_2O$ co-influx, increasing $P_i/P_o$ strongly increases $[glc_o]_{min}$. For $P_i$ = 1.04 $P_o$, $[glc_o]_{min}$ is already ~10 µM (*greater than* [glc$_i$] here) for rSGLT1. The location of the hexokinase glucose$_i$ $K_m$ is shown as a horizontal dashed line. Of course, the position of the surface depends also on the $E_{m,oi}$, [glc$_i$], and [$Na_i^+$] values, among other quantities. For example, making $\Delta G_{Na}(infl)$ less negative (say, by increasing [$Na_i^+$]) would increase $[glc_o]_{min}$, all other factors being equal – a given $P_i/P_o$, for example.

Plausible water chemogenic $\Delta G_{H2O}(infl)$ valies (- 5 to 5 J/mole) are small compared with a typical barogenic magnitude ($2.58ln(P_i/P_o) = 2.58ln(1.03)$ = 76 J/mole), which favors efflux. Thus, it is relatively inconsequential whether

bioRxiv preprint doi: https://doi.org/10.1101/2024.04.17.589812; this version posted April 26, 2024. The copyright holder for this preprint (which was not certified by peer review) is the author/funder, who has granted bioRxiv a license to display the preprint in perpetuity. It is made available under aCC-BY-NC-ND 4.0 International license.



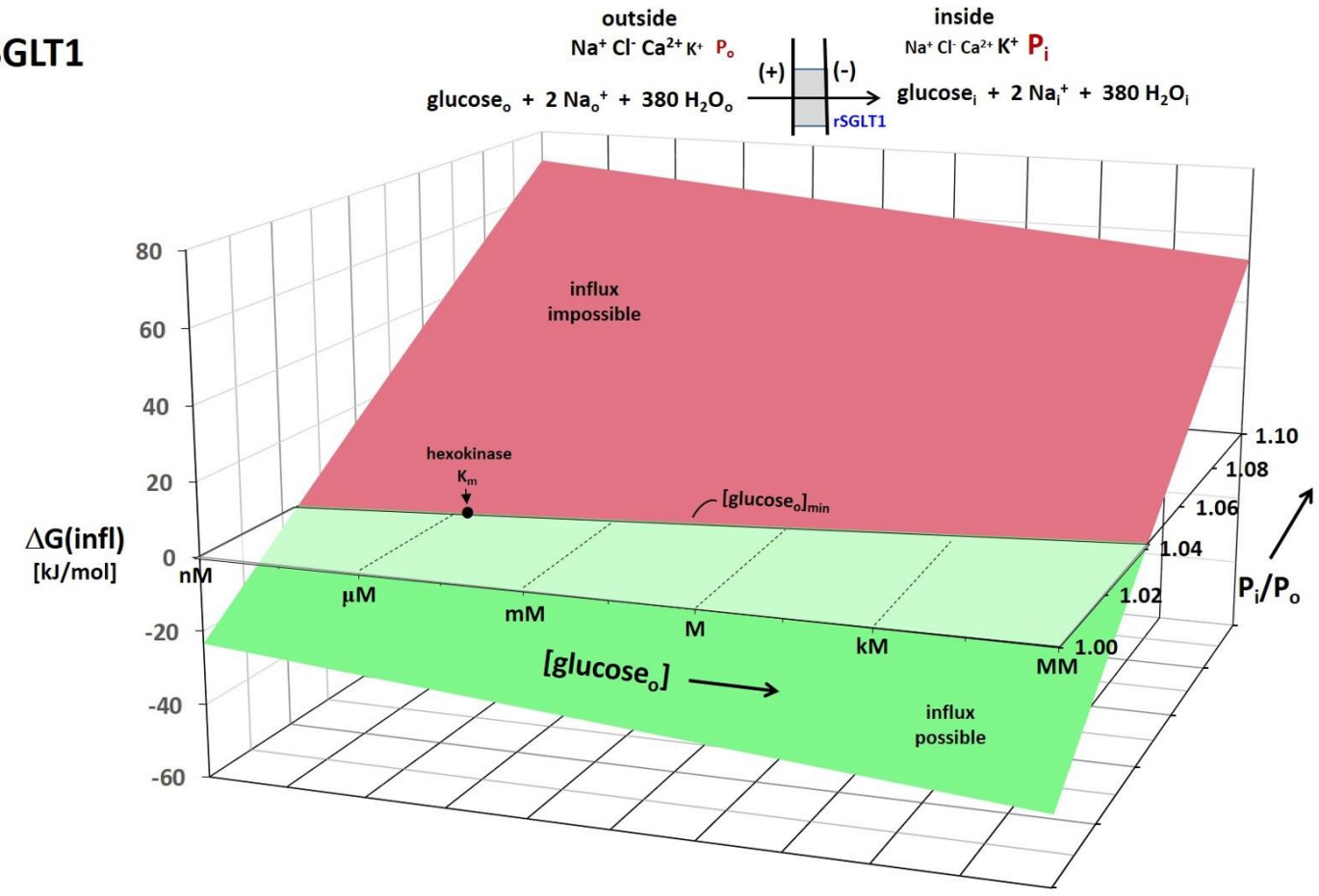


**Figure 4. A 3D plot for the rSGLT1 reaction.** The vertical axis measures the Gibbs free energy change (ΔG) for the influx direction shown, and calculated with Eq. (6). The logarithmic oblique axes plot the extracellular glucose concentration, [glucose$_o$], and the intracellular/extracellular hydraulic pressure ratio ($P_i/P_o$) over the experimentally measured range. For this calculation, the Table 1 concentrations and the Tables 2 and 3a free energy terms were used (chemogenic $\Delta G_{H2O}$(infl) = - 3 J/mole). The intracellular glucose concentration, [glucose$_i$], the membrane potential, $E_{m,oi}$, and $P_o$ were held fixed at 2 µM, - 91 mV, and 1 atm, respectively (T = 310 K). The surface is colored green when influx is thermodynamically possible and red when it is impossible. Thus, the intersection of the ΔG surface with the ΔG = 0 plane traces the trajectory of the ($P_i/P_o$)-dependence of the *minimum*, [glucose$_i$]$_{min}$, value. The value of the intracellular hexokinase $K_m$ (1.7 µM) for glucose$_i$ is indicated.

bioRxiv preprint doi: https://doi.org/10.1101/2024.04.17.589812; this version posted April 26, 2024. The copyright holder for this preprint (which was not certified by peer review) is the author/funder, who has granted bioRxiv a license to display the preprint in perpetuity. It is made available under aCC-BY-NC-ND 4.0 International license.



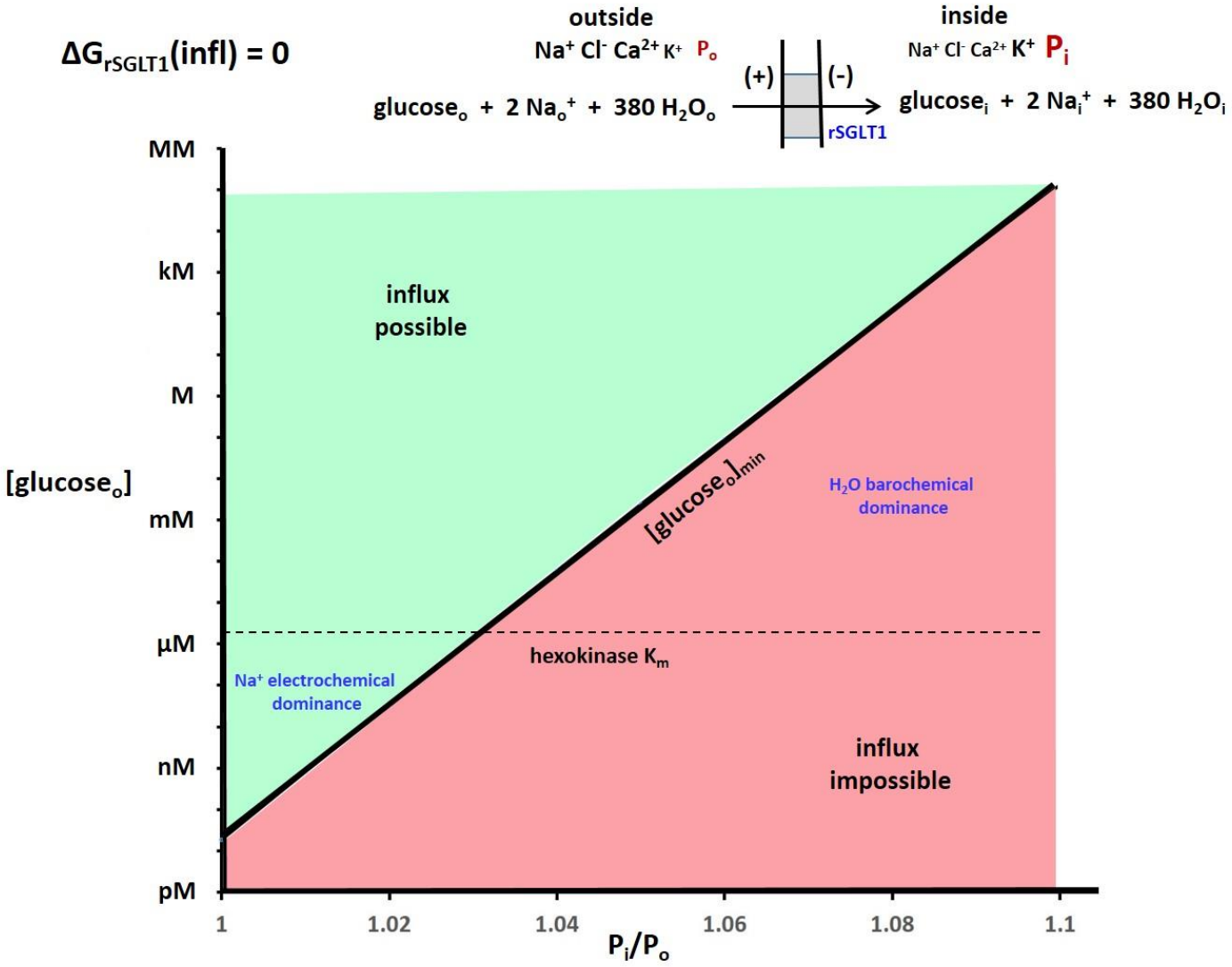


**Figure 5. The 2D plot of the Figure 4 $\Delta G_{rSGLT1}$(influx) = 0 plane.** The regions where the $Na^+$ electrochemical gradient dominate and the $H_2O$ barochemical gradient dominate are indicated. The dependence is so strong that small percentage changes of $P_i$ cause very large changes of the minimum [$glucose_o$] required for glucose uptake. The hexokinase $K_m$ for $glucose_i$ (1.7 µM) is indicated with a horizontal line.

bioRxiv preprint doi: https://doi.org/10.1101/2024.04.17.589812; this version posted April 26, 2024. The copyright holder for this preprint (which was not certified by peer review) is the author/funder, who has granted bioRxiv a license to display the preprint in perpetuity. It is made available under aCC-BY-NC-ND 4.0 International license.



water is in chemical equilibrium ($OsX_{H2O,i} = OsX_{H2O,o}$) or not. The larger steady-state water barochemical potential gradient is mostly barogenic.

Since it is likely almost all cells have $P_i$ 1.01 atm or greater, it seems that each of the Table 3a reactions will have similar behaviors. The water barochemical contributions provide crucial counterbalances for other influx transporters as well.

Though the GLUT family of glucose influxers lacks the large SGLT $Na^+$ electrochemical potential gradient favoring influx, it also has a smaller $H_2O$ barochemical force opposing influx when $P_i > P_o$: the GLUT $H_2O$ stoichiometries are smaller (Fig. 1). **Figure 6** contrasts the 2D plot of GLUT1 with that of rSGLT1 (from Fig. 5) and makes obvious for the SGLT family the $Na^+$ electrochemical dominance at small $P_i$ values and the $H_2O$ barochemical dominance at large $P_i$.

Glucose Uptake at Fixed [glucose$_o$]. For an alternative perspective, we take the extracellular glucose concentration, [$glc_o$], to be maintained at 5 mM (a large, but reasonable (68,69), value). With rSGLT1, if we fix $P_i$ = 1.05 $P_o$ and neglect water co-transport, ΔG remains negative until the intracellular glucose concentration, [$glc_i$], reaches the absurdly large value of 300 M. On the other hand, if we keep $P_i$ = 1.05 $P_o$ but retain the water co-transport, the reaction becomes unfavorable when [$glc_i$] reaches only 4.1 µM. More generally for rSGLT1 with $H_2O$ transport, **Figure 7** shows the ($P_i/P_o$)-dependence of $[glc_i]_{max}$, with [$glc_o$] fixed at 5 mM. The location of the hexokinase $glucose_i$ $K_m$ is shown as a horizontal dashed line. For such a plot, in the lower portion of the graph, the influx reaction is now possible (green), while it is impossible (red) in the upper portion. The maximum value of [$glc_i$] is greatly suppressed by increasing $P_i/P_o$.

For GLUT2 at $P_i$ = 1.04 $P_o$ and [$glc_o$] = 5 mM, [$glc_i$] could accumulate to 4.8 mM if there was no water co-influx, but only 110 µM with $H_2O$ co-influx.

Neurotransmitter Uptake and Clearance. There are considerable similarities of the rSGLT and excitatory amino acid transporter (EAAT1) influx reactions – with the exceptions of the $H_3O^+$ co-influx and $K_i^+$ co-efflux of the latter. $Glutamate^-$ influx is greatly aided by the $Na^+$ electrochemical gradient, but opposed by the $H_2O$ barochemical gradient. The analogous EAAT1 3D plot (not shown) is very similar to that for rSGLT (Fig. 4). However, the roles of these two reactions are quite different. While the purpose of rSGLT is mainly to deliver glucose into cells, that of EAAT1 is principally to clear $glutamate^-$ from synapses (*via* astrocytic uptake) after action potential transmission.

Now, besides $E_{m,oi}$ = - 91 mV as before, we fix *intracellular* [$glutamate_i^-$] at 1.4 mM, the $glutamate_i^-$ $K_m$ for glutamine synthetase (70), which converts astrocytic $glutamate_i^-$ to $glutamine_i$. **Figure 8** depicts the 2D $\Delta G_{EAAT1}(infl) = 0$ plane of the unshown 3D plot. The vertical axis measures log *extracellular* [$glutamate_o^-$], while the horizontal axis plots $P_i/P_o$. The intersection of the $\Delta G_{EAAT1}(infl)$ surface with the $\Delta G_{EAAT1}(infl) = 0$ plane traces

bioRxiv preprint doi: https://doi.org/10.1101/2024.04.17.589812; this version posted April 26, 2024. The copyright holder for this preprint (which was not certified by peer review) is the author/funder, who has granted bioRxiv a license to display the preprint in perpetuity. It is made available under aCC-BY-NC-ND 4.0 International license.



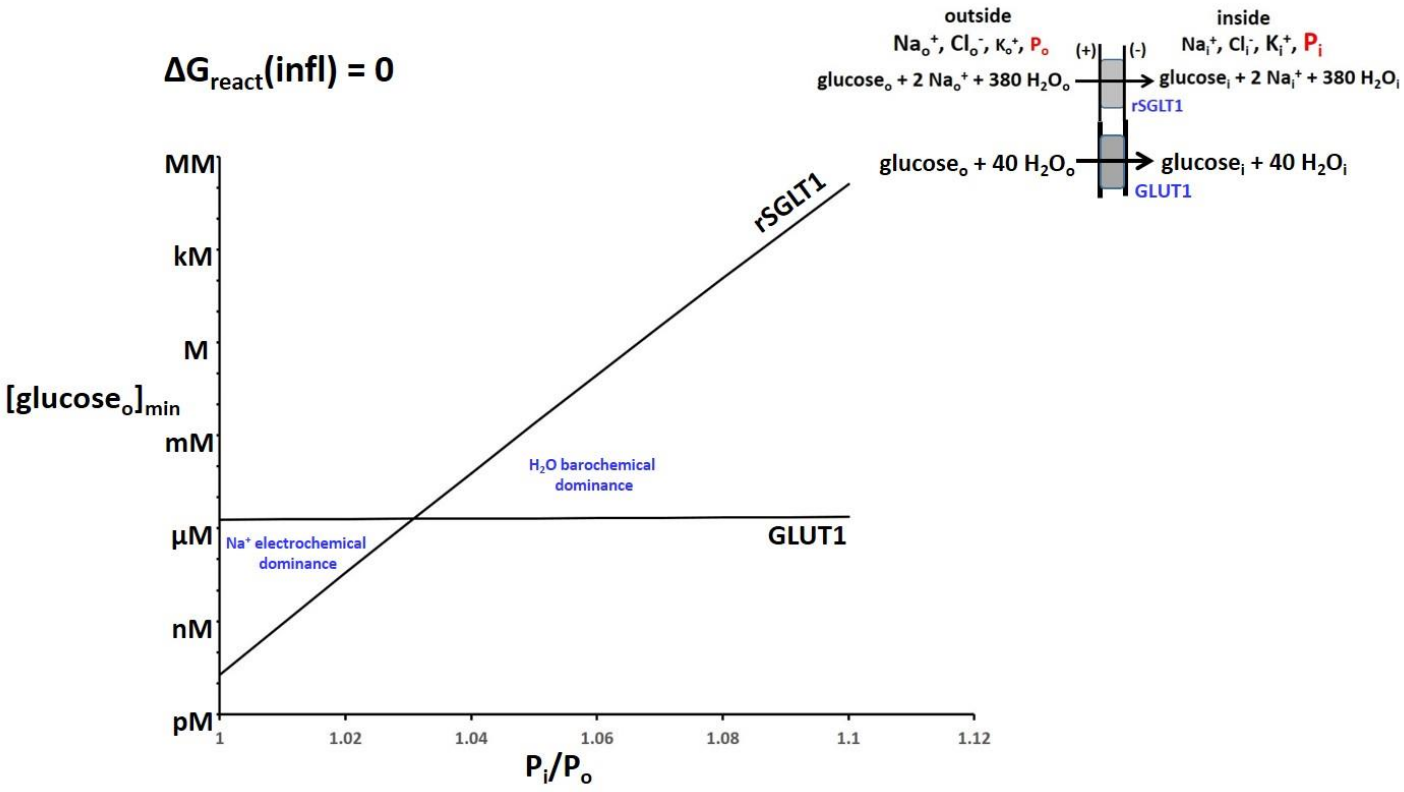


**Figure 6. The ($P_i/P_o$)-dependences of $[glucose_o]_{min}$ for rSGLT1 (from Fig. 5) and for GLUT1.** Equation (4) was used, with the intracellular glucose concentration, $[glucose_i]$, the membrane potential, $E_{m,oi}$, and $P_o$ held fixed at 2 μM, -91 mV, and 1 atm, respectively (T = 310 K). The regions of $Na^+$ electrochemical and $H_2O$ barochemical dominance are very evident. Influx through the rSGLT1 transporter is much more sensitive to $P_i/P_o$ than that (barely noticeable) through the GLUT1 transporter. This is due to the much greater water stoichiometry of the former (Fig. 1).

bioRxiv preprint doi: https://doi.org/10.1101/2024.04.17.589812; this version posted April 26, 2024. The copyright holder for this preprint (which was not certified by peer review) is the author/funder, who has granted bioRxiv a license to display the preprint in perpetuity. It is made available under aCC-BY-NC-ND 4.0 International license.



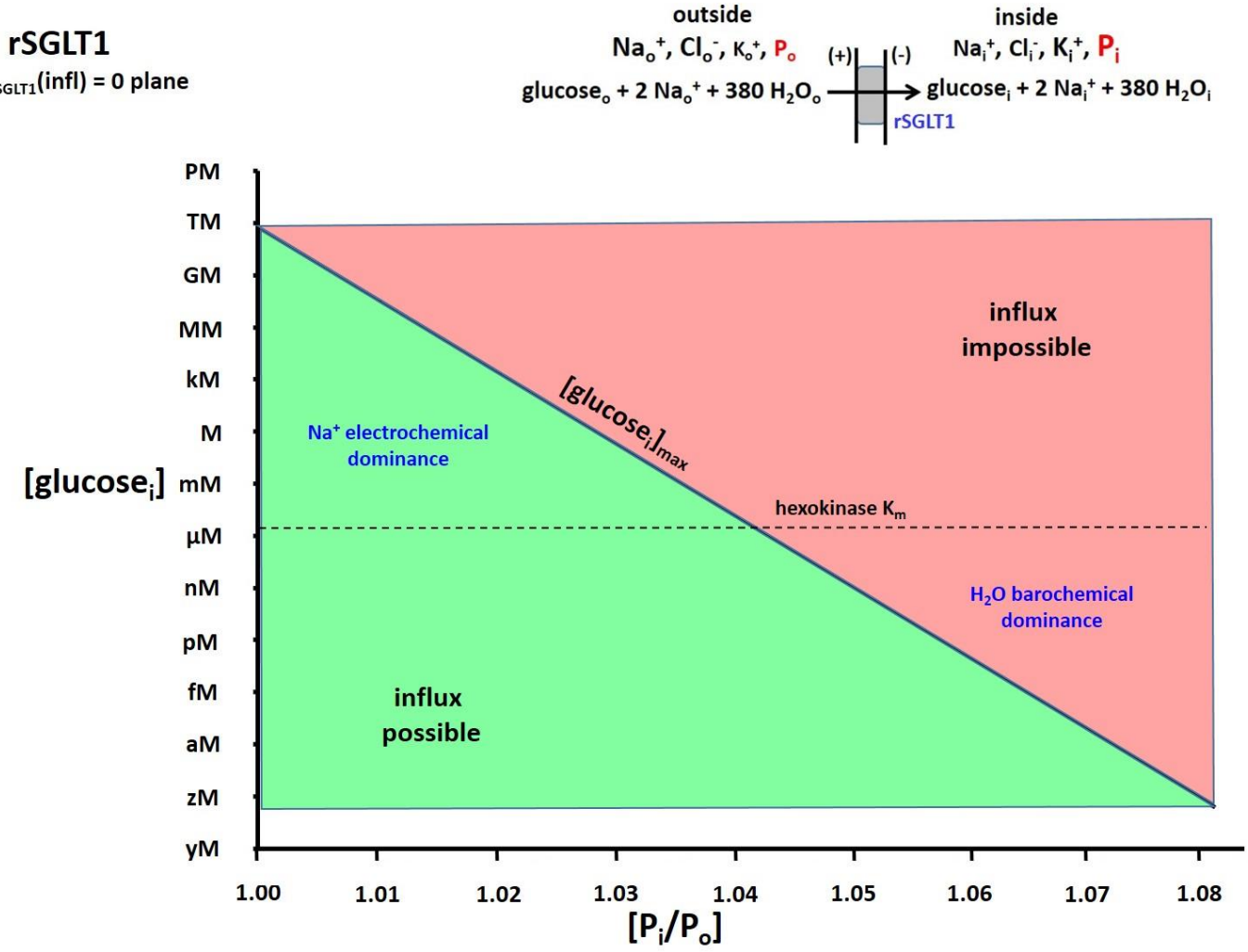


**Figure 7. The 2D plot of the $\Delta G_{rSGLT1}$(influx) = 0 plane from a 3D plot similar to Figure 4.** Equation (6) was used and, in this case, the *extracellular* glucose concentration, [glucose$_o$], the membrane potential, $E_{m,oi}$, and $P_o$ were held fixed at 5 mM, -91 mV, and 1 atm, respectively (T = 310 K). The surface is colored green when influx is thermodynamically possible and red when it is impossible. Thus, the intersection of the ΔG surface with the ΔG = 0 plane traces the trajectory of the ($P_i/P_o$)-dependence of the (in this case) *maximum* intracellular glucose$^-$ concentration, [glucose$_i$]$_{max}$, value allowing uptake. The $K_m$ value of the cytoplasmic hexokinase for glucose$_i$ (1.7 μM) is indicated with a horizontal dashed line. It is clear when $P_i$ is small, tremendous values of [glucose$_i$] are allowed, which would easily saturate hexokinase. However, this is not the case when $P_i$ is only a few percentage points greater.

bioRxiv preprint doi: https://doi.org/10.1101/2024.04.17.589812; this version posted April 26, 2024. The copyright holder for this preprint (which was not certified by peer review) is the author/funder, who has granted bioRxiv a license to display the preprint in perpetuity. It is made available under aCC-BY-NC-ND 4.0 International license.



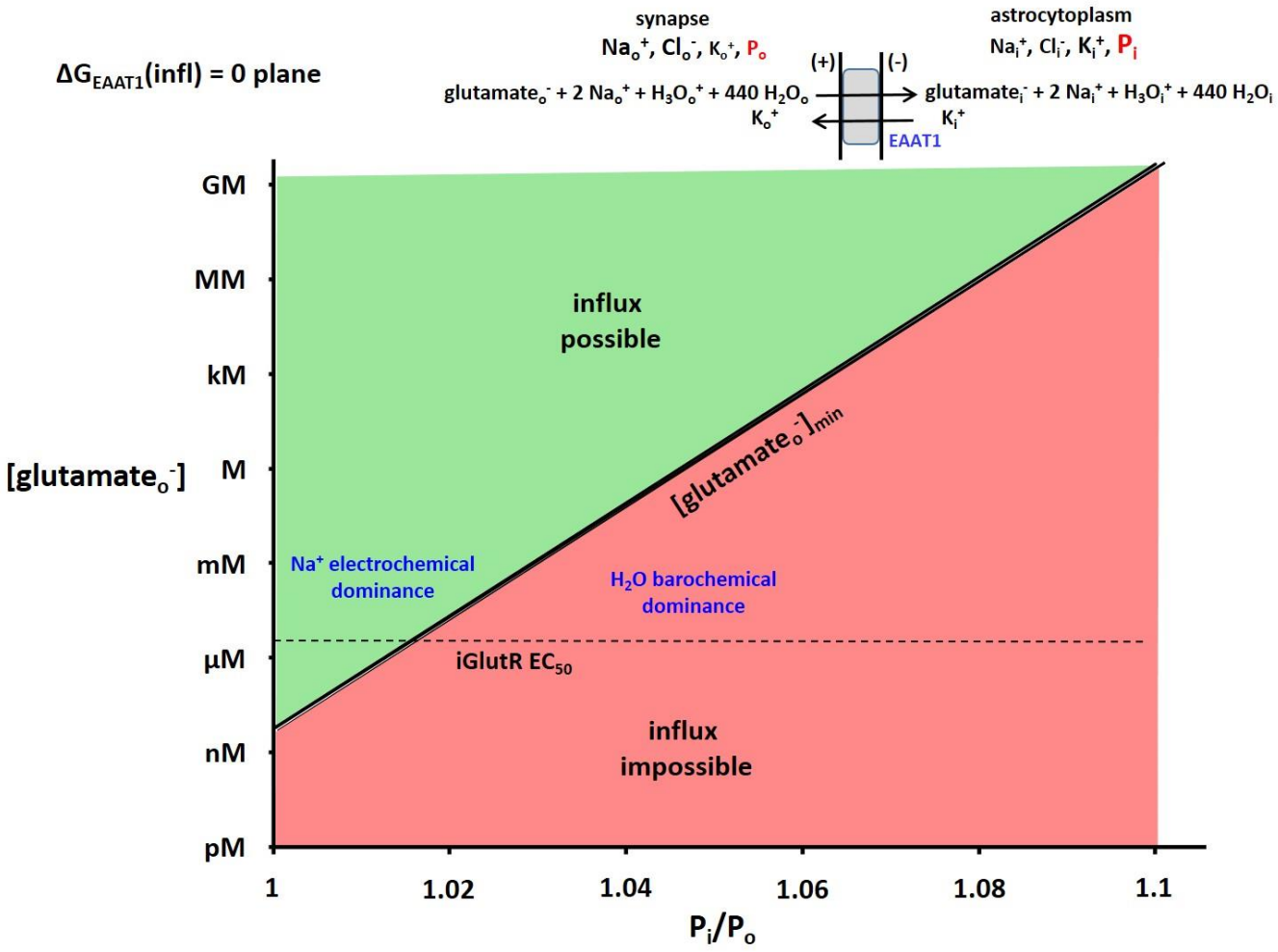


**Figure 8. The 2D plot of the $\Delta G_{EAAT1}$(influx) = 0 plane from the 3D plot analogous to Figure 4.** The (in this case) astrocytic glutamate$^-$ concentration, [glutamate$_i^-$], the membrane potential, $E_{m,oi}$, and $P_o$ were fixed at 1.4 mM (the $K_m$ value for glutamine synthetase), -91 mV, and 1 atm, respectively (T = 310 K). The surface is colored green when influx is thermodynamically possible and red when it is impossible. Thus, the intersection of the ΔG surface with the ΔG = 0 plane traces the trajectory of the ($P_i/P_o$)-dependence of the *minimum* synaptic glutamate$^-$ concentration, [glutamate$_o^-$]$_{min}$, value required for astrocyte uptake. The $EC_{50}$ value of the iGlutR receptor for synaptic glutamate$_o^-$ (2.3 μM) is indicated with a horizontal dashed line. It is clear glutamate$_o^-$ is well-cleared from the synapse when $P_i$ is small, and not when $P_i$ is only a few percentage points greater. In the latter case, the receptors would be saturated, and synaptic transmission would be interrupted.

bioRxiv preprint doi: https://doi.org/10.1101/2024.04.17.589812; this version posted April 26, 2024. The copyright holder for this preprint (which was not certified by peer review) is the author/funder, who has granted bioRxiv a license to display the preprint in perpetuity. It is made available under aCC-BY-NC-ND 4.0 International license.



the trajectory of the logarithm of the *minimum* glutamate$_o^-$ concentration ([glutamate$_o^-$]$_{min}$) necessary to initiate influx, as a function of $P_i/P_o$. Though strictly bi-exponential, the plot is almost a single exponential function (the exponential nature of the $P_i/P_o$ axis is very weak). For a member of the ionotropic glutamate receptor (iGlutR) family, the position of the L-glutamate$_o^-$ $EC_{50}$ value, 2.3 µM (71), is shown as a horizontal dashed line.

There is an influxer for which representative concentrations for all substrates are found in Table 2. $K_o^+$ influx *via* NKCC1 is not affected by the concentration of a metabolite substrate.

Inclusion of the effects of $E_{m,oi}$ and $\Delta G_{Na}$ variation would increase the dimensionalities of Figure 4-type plots. Making $\Delta G_{Na}$(infl) less negative, for example, would (non-linearly) shift the lines to the left in Figs. 5-8. Making $E_{m,oi}$ less negative (by increasing [$K_o^+$] or by [$K_i^+$] reduction) should do the same. In this paper, however, we focus on the novel (and large) effects of $P_i$ variation, consequent to water co-transport.

Efflux Reactions. The $\Delta G_{transporter}$(effl) values for the normal *efflux* reactions (II, I, or both, in Figs. 1,2) are found in **Table 3b** (again, $E_{m,oi}$ is fixed at – 91 mV). (Note: the calculations are for ΔG(effl), not ΔG(infl).) In contrast to the Table 3a influx reactions, except for that of KCC4 the other efflux reactions are unfavorable at $P_i/P_o$ = 1.00 (blue). But, they are made much more favorable as $P_i/P_o$ increases (red), because of water co-efflux.

There is an efflux reaction for which representative concentrations for all substrates are found in Table 2; KCC4, the [$K^+$,$Cl^-$,500$H_2O$] effluxer. For this, we see the efflux favorability is greatly enhanced by water co-efflux, even though it is slightly favorable even w/o $H_2O$ co-transport. Thus, it will always operate in efflux mode. $K_i^+$ efflux *via* KCC4 is not limited by the concentration of a metabolite substrate.

We focus on the lactic acid exporter, MCT1. The reaction is unfavorable when $P_i/P_o$ = 1.00, $\Delta G_{MCT1}$(effl) = 8.5 kJ/mole (blue), but very favorable, - 58 kJ/mole (red), when $P_i/P_o$ = 1.05. Again, this is due to $H_2O$ co-efflux. At $P_i/P_o$ = 1.05 atm, the [$lac_o^-$]/[$lac_i^-$] ratio could reach only two without water, but can attain 3 x $10^{10}$ with the 500 $H_2O$ molecules co-effluxed.

bioRxiv preprint doi: https://doi.org/10.1101/2024.04.17.589812; this version posted April 26, 2024. The copyright holder for this preprint (which was not certified by peer review) is the author/funder, who has granted bioRxiv a license to display the preprint in perpetuity. It is made available under aCC-BY-NC-ND 4.0 International license.



## DISCUSSION:

**Biochemical Roles for Water Co-Transport.** The analyses above suggest co-transported water can exert significant thermodynamic effects on its process *via* the cytoplasmic pressure ($P_i$). We elaborate some examples.

Figure 1 Glucose Influxers.

Small [glucose$_o$]. Commonly, the SGLT transporter family is thought of in terms of its potential for catalyzing glucose influx against its concentration gradient, chemogenic $\Delta G_{glc}$(infl) (72,73). However, Figs. 5 and 6 show this is true only when the $P_i$ value is relatively small. For rSGLT1, "uphill" glucose influx is impossible for any $P_i$ above ~1.03 $P_o$. A 1 % $P_i$ increase to 1.04 atm requires a [glc$_o$] value of at least ~10 µM for influx. This is five times *larger than* the 2 µM [glc$_i$] fixed for Figs. 5-6. Perhaps cells using exclusively SGLT transporters always have small $P_i$ values. Maybe $P_i$ fluctuation serves to control glucose influx. The GLUT family of transporters, with its smaller $H_2O$ stoichiometries (Fig. 1), does not suffer this severe ($P_i/P_o$)-dependence (Fig. 6). For GLUT1, the $H_2O$/glucose transport ratio is much smaller than for rSGLT1, and its [glc$_o$]$_{min}$ value is almost $P_i$-insensitive (Fig. 6). Perhaps cells with larger $P_i$ values, and in situations with smaller [glc$_o$] values, employ GLUT enzymes. On the other hand, if $P_i$ values are small, cells with SGLT transporters will take up glucose at smaller [glc$_i$] values than cells with GLUT transporters. When rSGLT1 $P_i$ is small, small [glc$_o$] can insure sufficient [glc$_i$]. Also, when $P_i$ is small, besides carrying glucose uphill, SGLT transporters are "pumping" water up a barochemical hill. They are maintaining the $H_2O$ barochemical steady-state.

Large [glucose$_o$]. If there is a situation where extracellular glucose is maintained at a relatively large value (*e.g.*, 5 mM), the role of $P_i$ can be viewed differently. Setting $P_i = P_o$, or ignoring co-transported water, would allow absurdly large [glc$_i$]$_{max}$ values for cells with SGLT enzymes (Fig. 7). This would surely amount to a sugar overload. Even if that was not cytotoxic, it could cause cells in a tissue to partake differentially of any available glucose charge – some cells initially reached by a bolus taking up more (or even all) sugar than others. This would mean a heterogeneous cellular [glc$_i$] spatial distribution. However with $H_2O$ co-transport, representative experimental $P_i$ values (say, 4% larger than $P_o$) suppress the [glc$_i$]$_{max}$ value to near the hexokinase $K_m$, 1.7 µM for glucose (Fig. 7). Cells with even larger $P_i$ values will take up less glucose than those with smaller $P_i$. For rSGLT1 when $P_i/P_o$ = 1.05 and [glc$_o$] = 5 mM, [glc$_i$]$_{max}$ is near 1 nM, insufficient for metabolism. With no $H_2O$ co-transport, [glc$_i$]$_{max}$ would increase more than ten orders of magnitude; many orders greater than the hexokinase $K_m$ for glucose.

For a given extracellular glucose concentration, cells with exclusively GLUT transporters will take up more glucose than cells with exclusively SGLT enzymes at larger $P_i$ values. Perhaps GLUT transporters are found in cells with larger $P_i$ values also in environments where [glc$_o$] is large.

As shown in Fig. 1, both SGLT and GLUT transporters deliver glucose. It is interesting a switch from GLUT1- to SGLT-mediated cellular glucose uptake during lung cancer progression has been reported (20).

bioRxiv preprint doi: https://doi.org/10.1101/2024.04.17.589812; this version posted April 26, 2024. The copyright holder for this preprint (which was not certified by peer review) is the author/funder, who has granted bioRxiv a license to display the preprint in perpetuity. It is made available under aCC-BY-NC-ND 4.0 International license.



More generally, GLUT1 expression (along with other genetic changes) is found to promote the cancer cell Warburg State (74). However, among these families, only the GLUTs transport the $^{18}$FDG-PET tracer, (2-fluorodeoxyglucose) 2-FDG (20). This produces an interpretation problem for the metabolic rate of glucose uptake and consumption determined by quantitative $^{18}$FDG-PET.

Because of $H_2O$ co-transport, cells seem never allowed much steady-state free glucose. The role of water co-influx, common to all the glucose influxers [hSGLT1, rSGLT1, GLUT1, GLUT2], appears dominant in controlling [$glc_i$]. It seems water co-transport *via* an SGLT generally guarantees a [$glc_i$] near the hexokinase $K_m$ for glucose. Glucose is effectively metabolized immediately upon entering the cell. This protects cells from too much glucose, and tissues from excessive cellular glucose uptake inequality. A large ([$glc_o$] - [$glc_i$]) difference makes [$glc_i$] hard to measure, even with modern methods (47). Also, $glc_i$ likely does not contribute to the glucoCEST NMR signal (75,76). On the other hand, GLUT1 generally keeps [$glc_i$] near [$glc_o$] (Fig. 6). (GLUT2 will keep it somewhat smaller.)

Figure 1 Neurotransmitter Influxers: astrocyte uptake / synaptic clearance.

Similar considerations must also obtain for the Table 3a influx reactions of the principal excitatory and inhibitory neurotransmitters $glutamate_o^-$ and $GABA_o$, respectively. Once inside the astrocyte, these must be processed immediately by their metabolizing enzymes. EAAT1 (Fig. 8) and GAT1 will not allow them to build-up. (Note: for EAAT1, $Z_{glt}$ = - 1, and there are $H_3O_o^+$ co-influx and $K_i^+$ co-*efflux* terms (21).)

However, an even more crucial aspect of the EAAT and GAT roles is the effective clearance of neurotransmitter species from synaptic junctions in time to enable the next action potential. Figure 8 shows this for EAAT1 and $glutamate_o^-$. It is clear the astrocyte $P_i$ must be relatively small (< 1.02 atm) to ensure [L-$glutamate_o^-$] does not much exceed 2.3 µM, its $EC_{50}$ value for the iGlutR receptor enzyme. At the same time, the astrocyte $P_i$ must be large enough (1.035 atm) to ensure astrocytosolic [L-$glutamate_i^-$] does not much exceed 1.4 mM, its $K_d$ value for glutamine synthetase (analogous to Fig. 7). The large $H_2O$ stoichiometries for EAAT1 (and GAT1) transport (similar to that of rSGLT1, Fig. 1) guarantee high sensitivity to astrocyte $P_i$.

The astrocytic uptake of synaptic $glutamate^-$ is particularly interesting. If astrocyte $P_i/P_o$ is even ~1.03, [$glutamate_o^-$] would have to reach ~100 µM (almost two orders of magnitude *over* 2.3 µM) to initiate uptake (Fig. 8). This could be sufficient to saturate iGlutR, and quench further synaptic transmission. Perhaps this is a physicochemical mechanism whereby astrocytes serve as "gatekeepers" for synaptic activity. Increases of $P_i$ to only 3 or 4% above $P_o$ could allow receptor saturation, and the interruption of neuronal firing. Very small astrocyte $P_i$ fluctuations could enable or disable synaptic function. For excitatory glutamatergic synapses this means turning off or on neural *excitation*. A glance at the Fig. 1 GAT1 influx stoichiometry indicates very similar considerations would obtain for GABAergic

bioRxiv preprint doi: https://doi.org/10.1101/2024.04.17.589812; this version posted April 26, 2024. The copyright holder for this preprint (which was not certified by peer review) is the author/funder, who has granted bioRxiv a license to display the preprint in perpetuity. It is made available under aCC-BY-NC-ND 4.0 International license.



synapses. In that case, neuronal *inhibition* could be halted by increased intra-astrocyte pressures – resulting in increased *excitation*.

Astrocyte swelling, a sign of possible $P_i$ change, has been implicated in the glymphatic processes occurring during sleep (commentary (77)). Also, it has been suggested some therapeutic interventions can disturb the glutamate$^-$/glutamine cycle leaving interstitial glutamine, which can act as a nutrient for brain cancer cells (78). In non-neural cells, [glutamate$_i^-$] values can become very large, 64 mM (47). Perhaps this is because there is no glutamine synthetase.

The Figure 1 NKCC1 Influxer.

The function of NKCC1 (reviewed in (22)) is to effect cellular $K_o^+$ and $H_2O_o$ uptake against their respective chemical and barochemical gradients. Because of the huge $H_2O$ stoichiometry (Fig. 1), this process is predicted to be strongly $P_i$-dependent.

Figure 1 Effluxers.

For the Table 3b effluxers, each of the reactions are made significantly more favorable by increased intracellular pressure (only KCC4 is favorable when $P_i = P_o$, and NaDC1 requires $P_i/P_o > 1.05$). Again, this is due to the pressure effect on the free energy caused by the large numbers of co-transported $H_2O$ molecules.

We use the monocarboxylate transporter [MCT1] as an example. It's main role is ridding the cell of lactic acid build-up from glycolytic-type metabolism. This is common in cancer cells (the Warburg Effect). Lactic acid can be sufficiently cytotoxic that MCT1 inhibition has been considered as a cancer therapy (79). **Equation (7)** expresses

$$\Delta G_{MCT1}(effl) = \left[2.58ln\left\{\frac{[lac_o^-]}{[lac_i^-]}\right\} - 0.0965(-0.91) + 2.58ln\left\{\frac{P_o}{P_i}\right\}\right] + \left[2.58ln\left\{\frac{[H_3O_o^+]}{[H_3O_i^+]}\right\} + 0.0965(-0.91) + 2.58ln\left\{\frac{P_o}{P_i}\right\}\right] + 500\left[2.58ln\left\{\frac{OsX_{H2O,o}}{OsX_{H2O,i}}\right\} + 2.58ln\left\{\frac{P_o}{P_i}\right\}\right] \quad (7)$$

the free energy change for the lactic acid efflux reaction: the first, second, and third terms represent the lactate$^-$, $H_3O^+$, and $H_2O$ contributions, respectively. Taking the Table 1 $H_3O^+$ and $OsX_{H2O}$ concentrations, $E_{m,oi}$ = -0.91 mV, $\{P_o/P_i\}$ = {1/1.05} = 0.95, and letting $\Delta G_{MCT1}$(effl) = 0, we solve for the maximum $\{[lac_o^-]/[lac_i^-]\}$ value that can be achieved. We find $\{[lac_o^-]/[lac_i^-]\} = 2.6 \times 10^{10}$ when 500 $H_2O$ molecules are co-transported, compared with only 2 if there was no $H_2O$ co-transport. This ten order-of-magnitude increase insures essentially all lactic acid is expelled from the cell – because of the barochemical water contribution. Once again, water co-transport is protecting the cells – even if they are malignant. A consequence is the extracellular acidification common in tumors (79). This phenomenon is also found for other cell types (*e.g.*, muscle tissue cramping).

We now scrutinize the nature of intracellular hydraulic pressure ($P_i$).

bioRxiv preprint doi: https://doi.org/10.1101/2024.04.17.589812; this version posted April 26, 2024. The copyright holder for this preprint (which was not certified by peer review) is the author/funder, who has granted bioRxiv a license to display the preprint in perpetuity. It is made available under aCC-BY-NC-ND 4.0 International license.



**The Nature of Intracellular Pressure.** It seems clear the crucial thermodynamic role played by co-transported water is effectuated by the pressure difference across the cell membrane. The intracellular pressure ($P_i$) is commonly considered "osmotic" in nature. That is, it is thought to result from the phenomenon of *water molecules* crossing the membrane. The simple first-order picture ($H_2O$ permeable; osmolytes ($Na^+$, $K^+$, $Cl^-$) impermeable in the $P_f$(p) sense) invokes *selective* water permeability, with influx and efflux becoming the same when ΔP ($\equiv P_i - P_o$) equals RT times the trans-membrane osmotic gradient (7): at T = 310 K, RT is 25.4 L•atm/mole. Strictly, osmotic effects are entropic in nature (the entropy of mixing (27)).

The first-order expression for the trans-cytolemmal osmotic gradient ($\Delta\pi_{oi}$) in terms of osmolyte concentrations is given in **Equation (8)**, where [osmolytes$_i$] and [osmolytes$_o$] are the intra- and extracellular concentrations,

$$\Delta\pi_{oi} = \pi_i - \pi_o = RT([osmolytes_i] - [osmolytes_o]) = 25.4([osmolytes_i] - [osmolytes_o]) \quad (8)$$

respectively. This equation assumes *ideal solutions* ((44), p 37; (80), p. 302 ff): *i.e.*, entropy only. In Eq. (8), the osmolyte concentrations are given on the osmolarity scale. We use the representative values listed in Table 1. There, total [osmolytes$_i$] = 0.379 OsM and total [osmolytes$_o$] = 0.289 OsM. (At such magnitudes, these are essentially identical to their *molal* concentrations. We neglect the tiny mOsM intracellular RNA, lipid, and DNA concentrations.) Inserting these into Eq. (8) yields $\Delta\pi_{oi}$ = 2.29 atm. With the Table 1 compartmental water contents, we can also estimate volume molal ($_V$m = OsM/$f_W$) osmolyte concentrations. We obtain: $_V m_i$ = 0.38/0.76 = 0.50 mole(osmolytes)/L(cell water), and $_V m_o$ = 0.29/0.82 = 0.35 mole(osmolytes)/L(extracellular water). Inserting these into Eq. (8) gives: $\Delta\pi_{oi}$ = 25.4 ($_V m_i$ - $_V m_o$) = 25.4(0.50 – 0.35) = 3.8 atm, an even greater value.

If there were only first-order mixing entropy contributions, $P_i$ would equal 2.3 or 3.8 atm at osmotic "equilibrium" (really steady-state; assuming $P_o$ = 1 atm). A molecular mechanism for selective water influx and efflux could be free (*i.e.*, unregulated) bidirectional aquaporin-mediated transport, as has been suggested (81). However, the largest experimental $P_i$ value (1.5 atm (66)) is 1.5 times smaller than even 2.3 atm. The most pertinent $P_i$ values (1.02 to 1.05; Figs. 4-8) are more than 2.2 times smaller. A ($P_i$ - $P_o$) of 1.03 would correspond to Δ[osmolytes] = 0.04 OsM (1.03/25.4). This is 2.5 times smaller than the 0.1 OsM value we estimate in Table 1. Of course, the Table 1 Δ[osmolytes] value is not found for any real cell. However, it is a reasonably representative magnitude: it is very unlikely to be less than 1.5 times any real value. If anything, 0.1 OsM may even be small (52). It is not clear any real cytoplasmic lipid bilayer membrane could even survive ΔP of 2.3 atm (the hydraulic pressure *ca.* 38 ft below sea level) if the *internal* pressure ($P_i$) is the greater, let alone 3.8 atm. Even if it could, a ΔP value of even 2.29 atm would yield a barogenic Eq. (8) term: ΔG(infl) = 2.58ln(2.29) = 2.14 kJ/mole. This is so large, it would dominate the values in Tables 2 - 4, and obliterate the realistic estimations of the last section.

bioRxiv preprint doi: https://doi.org/10.1101/2024.04.17.589812; this version posted April 26, 2024. The copyright holder for this preprint (which was not certified by peer review) is the author/funder, who has granted bioRxiv a license to display the preprint in perpetuity. It is made available under aCC-BY-NC-ND 4.0 International license.



Such first-order considerations carry the implicit assumption of solution *ideality*; no specific osmolyte/osmolyte molecular interactions. Osmotic pressure is generally considered one of the "colligative" properties: the identity of the osmolyte is irrelevant. This is why the mole fraction concentration scale, mOsX (or the related mOsm scale), for solution components is the most appropriate for osmotic considerations ((44), p. 56; (45), p.27; (46)). But, since the Table 1 osmolyte mOSM values are sufficiently small (in the absolute sense) that mOsm values can be used, this suggests their activity coefficients ($\gamma_{osmolyte}$, or $y_{osmolyte}$) are near unity. However, such reasoning does "fail to emphasize the departure from ideality indicated by the activity of the solute" ((45), p.29).

Furthermore, we see from Table 1 intra- and extracellular water mole fractions $OsX_{H2O,i} = 0.993$ and $OsX_{H2O,o} = 0.995$, respectively. $OsX_{H2O,i}$ is only 0.2% smaller than $OsX_{H2O,o}$, and each is nearly the value for pure water. Given this situation, it is not unreasonable to also assume the water activity coefficients are equal, $f_{H2O,i} = f_{H2O,o}$ (63). In **A.2**, we present calculations of $H_2O$ activities for surrogate interstitial and cytosolic solutions that support this contention. Table 2 shows inserting the calculated values $a_{H2O,i} = 0.994$ and $a_{H2O,o} = 0.995$ into Eq. (3) or (4), leads to a water chemogenic contribution to $\Delta G_{H2O}$(infl) of only ~3 J/mole favoring cellular water influx. Also, we showed above that chemogenic $\Delta G_{H2O}$(infl) =- 0.003 kJ/mole is counteracted by a $P_i/P_o$ ratio of only 1.001. This is only one tenth of a conservatively small typical intracellular pressure, $P_i/P_o = 1.01$ (27,66). This adds to the suggestion the entropic contribution to $P_i$ is actually small, usually less than 10%.

All these considerations indicate the mixing entropic contribution (- $T\Delta S_{H2O}$(infl)) to water $\Delta G_{H2O}$(infl) is small. By definition, a thermodynamically non-ideal solution means there is an enthalpic ($\Delta H_{H2O}$(infl)) contribution. A representative $P_i/P_o$ value of 1.05 corresponds to barochemical $\Delta G_{H2O}$(infl) = - 0.13 kJ/mole. A $P_i/P_o$ ratio of 1.001 implies ~90% $\Delta H_{H2O}$(infl); *i.e.*, - 0.12 kJ/mole. The conclusion must be that enthalpic ($\Delta H_{H2O}$(infl)) contributions dominate $P_i$. The aqueous solutions inside (and, for that matter, outside) cells deviate greatly from ideality. There are highly specific molecular interactions between the various solutes, and with water. It has long been known the "hydration" of biological solutes is extremely important for many different cellular processes (57-59). If the solute-interacting water entropy is smaller than in pure water, this could even give rise to a (not mixing) entropic driving force for *efflux*. Whatever the actual case, the intracellular osmolytes do not seem to lower the water "escaping tendency" nearly as much as the first-order osmotic pressure equation (8) would predict.

There is a long history of considering higher order contributions to Eq. (8) ((82), p. 210 ff; (83)). However, it is probably not realistic to expect an environment as complex as the intracellular *milieu* to be well-modeled as a homogeneous solution.

Recent reports suggest particular intracellular species contribute to regulating intracellular hydraulic pressure. These include: the mechanosensitive transcriptional regulator YAP (Yes-associated protein) (84), tropomyosins 1.6 and

bioRxiv preprint doi: https://doi.org/10.1101/2024.04.17.589812; this version posted April 26, 2024. The copyright holder for this preprint (which was not certified by peer review) is the author/funder, who has granted bioRxiv a license to display the preprint in perpetuity. It is made available under aCC-BY-NC-ND 4.0 International license.



2.1 (Tpm 1.6 and Tpm 2.1) (85), and the capsaicin-activatable transient receptor potential vanilloid 1 (TRPV1) cation channel, that interestingly, stimulates the Fig. 1 NKCC1 water co-influxer (86) as well as NKA. An especially intriguing proposal is that intracellular macromolecular polyanion electrostatic interactions dominate $P_i$, while allowing modulation by extracellular osmolality (52).

It may be often assumed tissue homeostasis means $\Delta\pi$ is zero, and is regulated to that point: *i.e.*, [osmolytes$_i$] = [osmolytes$_o$] in Eq. (8): *i.e.*, "*isosmolality*." However, the word "*isotonal*" (6) suggests only equal pressures, and is preferred. A 290 mOsm NaCl solution is often considered "*isotonic*." Bathing solutions hyper- or hypo-tonic relative to this cause *in vitro* cells (19) and *ex vivo* tissue cells (87) to shrink or swell due to *net* water efflux or influx, respectively. Bolus blood infusions of "*hypertonic*" solutions are used clinically to *transiently* open the blood-brain-barrier by shrinking capillary endothelial cells – and thus deliver otherwise non-extravasating therapeutic drugs to the cerebral parenchyma (88). In cell cultures and to some degree in perfused tissues, the investigator can specify and control [osmolytes$_o$]. When such a system reaches homeostasis, a common presumption may be that [osmolytes$_i$] = [osmolytes$_o$]. From this, it is usually assumed [osmolytes$_i$] ≈ 0.3 OsM, the Table 1 [osmolytes$_o$] value (52). However, our estimated [osmolytes$_i$] ≈ 0.4 OsM (Table 1) indicates this may be rarely (never) true.

Likely further evidence of cytoplasmic non-ideality is that different tissues seem to require different bathing solution osmolalities to achieve isotonicity. While ~320 mOsm suffices for the retina and olfactory bulb, almost 600 mOsm is required for cerebral cortex (87). Inhibition of NKA causes cortical cells to swell considerably; *i.e.*, a net category B water influx (89).

Whatever the actual $P_i$ physicochemical nature, the calculations in the last section remain valid because they employ experimental $P_i$ values.

**Aquaporin Role in Cellular Homeostasis.** The specific water-transporting membrane aquaporin (AQP) molecules are found in almost all tissues (6,90,91). Like all the Fig. 1 transporters, they are capable of catalyzing category B unidirectional (flux, $P_f$-type) or category A bidirectional (exchange, $P_d$-type) water transport. The famously large "single channel" AQP4 water volume flux, 0.25 fL/s/AQP4 (8.3 $H_2O$ molecules/ns/AQP4), was determined at 10°C and with a very large 4.4 atm osmotic gradient (92). Like all $P_f$ measurements, this is derived from the *asymptotic* volume change when transport is initiated away from osmotic "equilibrium." However, AQP efficiency is minimal when there is no pressure gradient ($\Delta P = 0$) (37), *i.e.*, the $P_d$-type condition. This is consistent with molecular considerations (the water single-file nature of the AQP channel structure (30) is not optimal for exchange). Thus, AQP's by themselves have been thought of as intrinsically *passive* transporters. They can facilitate very large *net* water influxes or effluxes, but only when the latter are driven by independent forces. Thus, though their involvement in non-homeostatic cell swelling or shrinking has been widely investigated (6,90,91), their roles in homeostasis has been less clear. We are not aware a "single channel" category A exchange magnitude has ever been experimentally determined.

bioRxiv preprint doi: https://doi.org/10.1101/2024.04.17.589812; this version posted April 26, 2024. The copyright holder for this preprint (which was not certified by peer review) is the author/funder, who has granted bioRxiv a license to display the preprint in perpetuity. It is made available under aCC-BY-NC-ND 4.0 International license.



The results presented here suggest there is thermodynamic (metabolic) energy stored in tissue water compartmentalization itself, helping maintain the system in homeostasis. Thus, we have inserted AQPs explicitly into the active trans-membrane water cycling (AWC) scheme, rate-limited by $^{c}MR_{NKA}$ (Fig. 2). Since AWC is, by definition, homeostatic, $MR_{H2O}$(infl) = $MR_{H2O}$(effl). However, it is unlikely AQP's contribute equally to water influx and efflux. As stated above, if ΔP was actually osmotic in nature, unregulated dominant AQP activity would lead to ΔP values many times those measured. Thus, it is likely $MR_{AQP}$(infl) ≠ $MR_{AQP}$(effl).

In cell suspensions (and *in vivo*) astroglial aquaporin AQP4 expression has been shown to contribute to category A water exchange (81). Furthermore, studies with human C6 glioma (cancer) cell suspensions and TGN020 (a specific AQP4 inhibitor) are informative. The $k_{io}$ rate constant ratios ($^{TGN020}k_{io}$)/($^{C6}k_{io}$) is 0.69, while ($^{ouabain}k_{io}$)/($^{C6}k_{io}$) is 0.65 (81). Inhibiting water exchange with extracellular TGN020 reduces $k_{io}$ to the same extent as inhibiting it with extracellular ouabain, the specific NKA inhibitor. This indicates AQP4 contributes to AWC. Cancer cells in suspension may not be in the Warburg state (2,4).

The metabolite influxers (Fig. 1) can provide significant $MR_{H2O}$(infl) values. The cellular glucose consumption rate, $MR_{glc}$(consump), has been determined to be 38 μM(glc)/s/cell for murine kidney epithelial cells (47) and for brain tissue cells, assuming reasonable cell density and volume values (68). The glucose influx rate, $MR_{glc}$(infl) must be at least $MR_{glc}$(consump). But GLUT1 and rSGLT1 have different stoichiometries (Fig. 1). Thus, $MR_{H2O}$(infl) would range from $1.8x10^9$ to $17x10^9$ $H_2O$/s/cell for 2pL cells with, respectively, exclusively GLUT1 or exclusively rSGLT1 transporters. Using the ratio of the glutamate$^-$-to-glutamine conversion flux, $MR_{glu\text{-}gln}$(cycle) to $MR_{glc}$(consump) (93), we estimate $MR_{H2O}$(infl) provided by the EAAT1 transporter to be $4 \times 10^7$ $H_2O$/s/cell for a 2 pL astrocyte. This would be in addition to $MR_{H2O}$(infl) provided by a glucose influxer.

Some so-called "metabolic water" is generated within the cell after glucose is imported. However, there are at most six $H_2O$ molecules produced per glucose molecule metabolized, depending on the glycolysis and oxidative phosphorylation proportions (94). This is small when compared with even the smallest Fig. 1 glucose influxer $H_2O$ stoichiometries.

Our most recent estimate of brain x, the $MR_{H2O}$(AWC)/$MR_{NKA}$ ratio, is > $10^6$ (2). We opined "such large stoichiometries suggest aquaporin participation in active trans-membrane water cycling." Given the large cellular water influx rates, and the $P_i > P_o$ pressure gradient, it seems likely $MR_{AQP}$(effl) > $MR_{AQP}$(infl). That is, in homeostasis AQP is likely mainly catalyzing water *efflux*. It is working in parallel with the KCC effluxer. This is why we indicate the inhibitor blocking $MR_{AQP}$(effl) in Fig. 2.

Water should be considered a substrate for active trans-membrane water cycling. It has thermodynamic consequences. If it turns out NKA itself has its own water stoichiometry, AQPs could be then considered as also

bioRxiv preprint doi: https://doi.org/10.1101/2024.04.17.589812; this version posted April 26, 2024. The copyright holder for this preprint (which was not certified by peer review) is the author/funder, who has granted bioRxiv a license to display the preprint in perpetuity. It is made available under aCC-BY-NC-ND 4.0 International license.



844 secondary active enzymes. If not, they are only tertiary active transporters – sharing water as a substrate
845 with only the secondary active water co-transporters.

846 An interesting analogy with potassium ion-specific channels (PCs) (reviewed in (29); (95)) might obtain. It is
847 thought the formally "passive" $K_i^+$ efflux through PCs dominates the production of $E_{m,oi}$. The idea is $K_i^+$ efflux driven
848 by the chemogenic term proceeds until the latter is balanced by the electrogenic term (Table 2), which actually requires
849 very few effluxed $K^+$ ions. After that, an "electrochemical" steady-state condition is reached, and *homeostatic* $K_i^+$ efflux
850 is synchronized with ${}^cMR_{NKA}$. If it is water transport that dominates the $P_i$ value, perhaps there is an analogous $H_2O_i$
851 efflux driven by the barochemical gradient. This would tend to decrease $P_i$. However, diminished $P_i$ would allow
852 the $Na^+$ electrochemical gradient a greater role. This would tend to increase the water co-influxes of the many
853 transporters that also bring in $Na^+$ (*e.g.*, NKCC- and SGLT-catalyzed influxes; Figs. 1-8), which would tend to increase $P_i$.
854 This "feedback loop" would then establish an NKA-maintained *steady-state*, and AQP-catalyzed water efflux is also
855 synchronized with ${}^cMR_{NKA}$. Thus, we have AQP playing a vital role in active trans-membrane water cycling (Fig. 2).

856 A trans-membrane pressure difference could also affect transporter *kinetics*. This is discussed in **A.3**.

857

bioRxiv preprint doi: https://doi.org/10.1101/2024.04.17.589812; this version posted April 26, 2024. The copyright holder for this preprint (which was not certified by peer review) is the author/funder, who has granted bioRxiv a license to display the preprint in perpetuity. It is made available under aCC-BY-NC-ND 4.0 International license.



## CONCLUSION:

The $Na^+$,$K^+$-ATPase (NKA) enzyme function has long been known to maintain $Na^+$ and $K^+$ in trans-membrane electrochemical *steady-states*, which are far from chemical *equilibria* ($[Na_i^+] = [Na_o^+]$, $[K_i^+] = [K_o^+]$). Here, we find metabolic energy released by NKA-catalyzed ATP hydrolysis is also required to maintain (and is thus stored in) in a trans-cytolemmal water barochemical steady-state. This is an inherent part of NKA function. An important difference from the $Na^+$ and $K^+$ cases is the trans-membrane water distribution is in (or near) chemical equilibrium ($[H_2O_i] \approx [H_2O_o]$). Crucially, the barochemical $H_2O$ steady-state is significant, and enzymatic water co-transport has very important thermodynamic metabolic consequences. Active trans-membrane water cycling does not represent a futile cycle.

bioRxiv preprint doi: https://doi.org/10.1101/2024.04.17.589812; this version posted April 26, 2024. The copyright holder for this preprint (which was not certified by peer review) is the author/funder, who has granted bioRxiv a license to display the preprint in perpetuity. It is made available under aCC-BY-NC-ND 4.0 International license.



## ACKNOWLEDGEMENTS:

The authors especially thank Professor Daniel Zuckerman for critical readings of manuscript drafts and very insightful suggestions, and Dr. August George for accomplishing initial calculations. They also thank Professors Joseph Ackerman, Valerie Anderson, James Balschi, James Bassingthwaighte, Cynthia Burrows, Deborah Burstein, Kieran Clarke, Ira Cohen, Michael Grabe, Fahmeed Hyder, Joanne Ingwall, Christopher Kroenke, Kenneth Krohn, Philip Kuchel, Xin Li, Daniel Liefwalker (for ref. (74)), Jeffrey Maki, Silvia Mangia, Richard Mathias, Anusha Mishra, William Rooney, Douglas Rothman, Suzanne Scarlatta, William Skach, and Mark Woods, and Drs. Joseph Armstrong, Mauro DiNuzzo, Bassam Haddad, Audrey O'Connor, and Gregory Wilson, and Messers. Eric Baetscher, Eric Baker, Brendan Moloney, and Joshua Schlegel for stimulating discussions.

Support:

- OHSU Brenden-Colson Center for Pancreatic Care; Sheppard (PI), Springer (PI)
- NIH UL1TR02369; Ellison, Morris (PIs); awarded by the Oregon Clinical and Translation Institute, Biomedical Innovation Program; Pike (PI)

## AUTHOR ROLES:

**CSS** conceived the approach, developed the theory, carried out the calculations, and drafted the manuscript.

**MMP** edited the manuscript drafts, with particular attention to the metabolic aspects.

**TMB** contributed calculations and edited the manuscript drafts, especially scrutinizing the theory.

## CONFLICTS OF INTEREST:

**CSS** and **TMB** are co-inventors on U.S. patent 11,728,038, "Activity MRI" (issued 15 August, 2023), which describes the MADI approach.

bioRxiv preprint doi: https://doi.org/10.1101/2024.04.17.589812; this version posted April 26, 2024. The copyright holder for this preprint (which was not certified by peer review) is the author/funder, who has granted bioRxiv a license to display the preprint in perpetuity. It is made available under aCC-BY-NC-ND 4.0 International license.



## REFERENCES:


1. C. S. Springer, E. M. Baker, X. Li, B. Moloney, G. J. Wilson, M. M. Pike, T. M. Barbara, W. D. Rooney, J. H. Maki, Metabolic activity diffusion imaging [MADI]: I. Metabolic, cytometric modeling and simulations. *NMR Biomed.* **36,** e4781 (2023).
2. C. S. Springer, E. M. Baker, X. Li, B. Moloney, G. J. Wilson, V. C. Anderson, M. K. Sammi, M. M. Pike, M. G. Garzotto, R. P. Kopp, F. V. Coakley, W. D. Rooney, J. H. Maki, Metabolic activity diffusion imaging [MADI]: II. Non-invasive, high-resolution human brain imaging of sodium pump flux and cell metrics. *NMR Biomed.* **36,** e4782 (2023).
3. J. J. Neil, J. J. H. Ackerman, Metabolic activity diffusion imaging (MADI): A new paradigm. *NMR in Biomed.* **36,** e4841 (2023).
4. J. Schlegel, E. Baker, S. Holland, J. Stoller, W. Packwood, X. Li, R. Barajas, C. Springer, M. Pike, Metabolic activity diffusion imaging [MADI] of rat brain glioma. *Proc. Int. Soc. Magn. Reson. Med.* **31,** 3924 (2023).
5. M. M. Pike, X. Li, E. Baetscher, T. M. Barbara, M. K. Sammi, A. A. Stevens, C. S. Springer, Does MADI detect temporal brain metabolic activity changes?" *Proc. Int. Soc. Magn. Reson. Med.* **31,** 5177 (2023).
6. R. E. Day, P. Kitchen, D. S Owen, C. Bland, L. Marshall, A. C. Conner, R. M. Bill, M. T. Conner, Human aquaporins: Regulators of transcellular water flow. *Biochim. Biophys. Acta* **1840,** 1492-1506 (2014). [doi.org/10.1016/j.bbagen,2013,09,033]
7. A. S. Verkman, Water permeability measurements in living cells and complex tissues. *J. Membrane Biol.* **173,** 73-87 (2000).
8. E. Zeuthen, A sensitive 'Cartesian Diver' balance. *Nature* **159,** 440-441 (1947).
9. O. Kedem, A. Katchalsky, Thermodynamic analysis of the permeability of biological membranes to non-electrolytes. *Biochim. Biophys. Acta* **27,** 229-246 (1958).
10. C. R. House, Water transport in cells and tissues. (Edward Arnold, London, 1974), p. 156.
11. S-T. Chen, C. S. Springer, Ionophore-catalyzed cation transport between phospholipid inverted micelles manifest in DNMR. *Biophys. Chem.* **14,** 375-388 (1981).
12. T. Conlon, R. Outhred, Water diffusion permeability of erythrocytes using an NMR technique. *Biochim. Biophys. Acta* **288,** 354-361 (1972).
13. C. S. Landis, X. Li, F. W. Telang, P. E. Molina, I. Pályka, G. Vétek, C. S. Springer, Equilibrium transcytolemmal water-exchange kinetics in skeletal muscle *in vivo*. *Magn. Reson. Med.* **42,** 467-478 (1999).
14. X. Li, W. D. Rooney, C. S. Springer, A unified magnetic resonance imaging pharmacokinetic theory: Intravascular and extracellular contrast reagents. *Magn. Reson. Med.* **54,** 1351-1359 (2005). [DOI 10.1002/mrm.20684]
15. C. S. Springer, Using $^{1}H_2O$ to measure and map sodium pump activity *in vivo*. *J. Magn. Reson.* **291,** 110-126 (2018). [doi.org/10.1016/j/jmr.2018.02.018]
16. B. P. Hills, P. S. Belton, NMR studies of membrane transport. *Ann. Reports NMR Spectroscopy* **21,** 99-159 (1989).
17. B. M. Denker, B. L. Smith, F. P. Kuhajda, P. Agre, Identification, purification, and partial characterization of a novel $M_r$ 28,000 integral membrane protein from erythrocytes and renal tubules. *J. Biol. Chem.* **263,** 15634-15642 (1988).
18. N. MacAulay, Molecular mechanisms of brain water transport. *Nat. Rev. Neurosci.* **22,** 326-344 (2021).
19. T. Zeuthen, Water-transporting proteins. *J. Membrane Biol.* **234,** 57-73 (2010). [DOI 10.1007/s00232-009-9216-y]
20. J. R. Barrio, S. C. Huang, N. Satyamurthy, C. S. Scafoglio, A. S. Yu, A. Alavi, K. A. Krohn, Does 2-FDG-PET accurately reflect quantitative *in vivo* glucose utilization. *J. Nucl. Med.* **61,** 931-937 (2020).
21. N. MacAulay, U. Gether, D. A. Klaerke, T. Zeuthen, Water transport by the human $Na^+$-coupled glutamate cotransporter expressed in *Xenopus* oocytes. *J. Physiol.* **530,** 367-378 (2001).

bioRxiv preprint doi: https://doi.org/10.1101/2024.04.17.589812; this version posted April 26, 2024. The copyright holder for this preprint (which was not certified by peer review) is the author/funder, who has granted bioRxiv a license to display the preprint in perpetuity. It is made available under aCC-BY-NC-ND 4.0 International license.




**22.** K. Kaila, T. J. Price, J. A. Payne, M. Puskarjov, J. Voipio, Cation-chloride cotransporters in neuronal development, plasticity and disease. *Nature Rev. Neurosci.* **15,** 637-654 (2014). [doi:10.1038/nrn3819]

**23.** A. W. Autry, J. W. Gordon, H-Y. Chen, M. LaFontaine, R. Bok, M. Van Criekinge, J. B. Slater, L. Carvajal, J. E. Villanueva-Meyer, S. M. Chang, J. L. Clarke, J. M. Lupo, D. Xu, P. E. Z. Larson, D. B. Vigneron, Y. Li, Characterization of serial hyperpolarized $^{13}C$ metabolic imaging in patients with glioma. *NeuroImage: Clin.* **27,** 102323 (2020).

**24.** R. Ye, A. S. Verkman, Simultaneous optical measurement of osmotic and diffusional water permeability in cells and liposomes. *Biochem.* **28,** 824-829 (1989).

**25.** X. Li, S. Mangia, J-H. Lee, R. Bai, C. S. Springer, NMR shutter-speed elucidates apparent population inversion of $^{1}H_2O$ signals due to active transmembrane water cycling. *Magn. Reson. Med.* **82,** 411-424 (2019). [DOI: 10.1002/mrm.27725]

**26.** Y. Zhang, M. Poirier-Quinot, C. S. Springer, J. A. Balschi, Active trans-plasma membrane water cycling in yeast is revealed by NMR. *Biophys. J*. **101,** 2833-2842 (2011). [DOI:10.1016/j.bpj.2011.10.035]

**27.** Y. Li, K. Konstantopoulos, R. Zhao, Y. Mori, S. X. Sun, The importance of water and hydraulic pressure in cell dynamics. *J. Cell. Sci.* **133,** jcs240341 (2020).

**28.** C. S. Springer, Measurement of metal cation compartmentalization in tissue by high resolution metal cation NMR. *Ann. Rev. of Biophys. and Biophys. Chem.,* **16**, 375-399 (1987).

**29.** C. Öster, K. Kendriks, W. Kopec, V. Chevelkov, C. Shi, D. Michl, S. Lange, H. Sun, B. L. de Groot, A. Lange, The conduction pathway of potassium channels is water free under physiological conditions. *Sci. Adv.* **5,** eeaw6756 (2019).

**30.** B. L. de Groot, H. Grubmüller, Water permeation across biological membranes: Mechanism and dynamics of aquaporin-1 and GlpF. *Science* **294,** 2353-2357 (2001).

**31.** R. Bai, C. S. Springer, D. Plenz, P. J. Basser, Brain active trans-membrane water cycling measured by MR is associated with neuronal activity. *Magn. Reson*. *Med.* **81,** 1280-1295 (2019). [DOI:10.1002/mrm.27473]

**32.** J. L. Adelman, C. Ghezzi, P. Bisignano, D. D. F. Loo, S. Choe, J. Abramson, J. M. Rosenberg, E. M. Wright, M. Grabe, Stochastic steps in secondary active sugar transport. *Proc. Nat. Acad. Sci.* **113,** E3960-E3966 (2016).

**33.** J. L. Adelman, Y. Sheng, S. Choe, J. Abramson, E. M. Wright, J. M. Rosenberg, M. Grabe, Structural determinants of water permeation through the sodium-galactose transporter vSGLT. *Biophys. J.* **106,** 1280-1289 (2014).

**34.** J. Li, S. A. Shaikh, G. Enkavi, P-C. Wen, Z. Huang, E. Tajkhorshid, Transient formation of water-conducting states in membrane transporters. *Proc. Nat. Acad. Sci.* **110,** 7696-7701 (2013).

**35.** S. Choe, J. M. Rosenberg, J. Abramson, E. M. Wright, M. Grabe, Water permeation through the sodium-dependent galactose cotransporter vSGLT." *Biophys. J.* **99,** L56-L58 (2010).

**36.** A. Watanabe, S. Choe, V. Chaptal, J. M. Rosenberg, E. M. Wright, M. Grabe, J. Abramson, The mechanism of sodium and substrate release from the binding pocket of vSGLT. *Nature* **468,** 988-991 (2010).

**37.** F. Zhu, E. Tajkhorshid, K. Schulten, Theory and simulation of water permeation in aquaporin-1. *Biophys. J.* **86,** 50-57 (2004).

**38.** S. Zhang, J. Zhou, Y. Zhang, T. Liu, P. Friedel, W. Zhou, S. Somasekharan, K. Roy, L. Zhang, Y. Liu, X. Meng, H. Deng, W. Zeng, G. Li, B. Forbush, M. Yang, The structural basis of function and regulation of neuronal cotransporters NKCC1 and KCC2. *Comm. Biol.* **4,** 226 (2021).

**39.** H. Ogawa, T. Shinoda, F. Cornelius, C. Toyoshima, Crystal structure of the sodium-potassium pump ($Na^+$,$K^+$-ATPase) with bound potassium and sodium." *Proc. Nat. Acad. Sci.* **106,** 13742-13747 (2009).

**40.** M. M. Pike, J. C. Frazer, D. F. Dedrick, J. S. Ingwall, P. D. Allen, C. S. Springer, T. W. Smith, $^{23}Na$ and $^{39}K$ nuclear magnetic resonance studies of perfused rat hearts. *Biophys. J.* **48,** 159-173 (1985).

**41.** A. L. Lehninger, "*Principles of Biochemistry*." (Worth Pub., New York, 1982), p. 571.

bioRxiv preprint doi: https://doi.org/10.1101/2024.04.17.589812; this version posted April 26, 2024. The copyright holder for this preprint (which was not certified by peer review) is the author/funder, who has granted bioRxiv a license to display the preprint in perpetuity. It is made available under aCC-BY-NC-ND 4.0 International license.




**42.** D. M. Bers, W. H. Barry, S. Despa, Intracellular $Na^+$ regulation in cardiac myocytes. *Cardiovas. Res.* **57,** 897-912 (2003).

**43.** A. A. Kadir, B. J. Stubbs, C-R, Chong, H. Lee, M. Cole, C. Carr, D. Hauton, J McCullagh, R. D. Evans, K. Clarke, On the interdependence of ketone body oxidation, glycogen content, glycolysis, and energy metabolism in the heart. *J. Physiol.* **601.7,** 1207-1224 (2023). [doi:10,1113/JP284270]

**44.** A. G. Marshall, "*Biophysical Chemistry: Principles, Techniques, and Applications*" (Wiley, New York, 1978).

**45.** R. A. Robinson, R. H. Stokes, in "*Electrolyte Solutions*" (Dover, Mineola, ed. 2nd rev., 1970).

**46.** M. J. Blandamer, J. B. F. N. Engberts, P. T. Gleeson, J. C. R. Reis, Activity of water in aqueous systems: A frequently neglected property." *Chem. Soc. Rev.* **34,** 440-458 (2005).

**47.** J. O. Park, S. A. Rubin, Y-F. Xu, D. Amador-Noguez, J. Fan, T. Shlomi, J. D. Rabinowitz, Metabolite concentrations, fluxes, and free energies imply efficient enzyme usage. *Nat. Chem. Biol.* **12,** 482-489 (2016).

**48.** O. S. Andersen, "Cellular electrolyte metabolism," in *Enclycopedia of Metalloproteins*, R. H. Kretsinger, V. N. Uversky, A. Permiakov, Eds. (Springer, 2013), pp. 580-587.

**49.** R. Milo, What is the total number of protein molecules per cell volume? A call to rethink some published values. *Bioessays.* **35,** 1050-1055 (2013). [DOI 10.1002/bies.201300066]

**50.** F. C. Neidhardt, H. E. Umbarger, in *Escherichia coli and Salmonella: Cellular and Molecular Biology*, F. C. Neidhardt, Ed. (Am. Soc. Microbiol. Press, New York, ed. 2, 1996), vol. 1, chapt. 3.

**51.** K. C. Vinnakota, J. B. Bassingthwaighte, Myocardial density and composition: A basis for calculating intracellular metabolite concentrations. *Am. J. Physiol. Heart Circ. Physiol.* **286,** H1742-H1749 (2004). [10.1152/ajpheart.00478-2003]

**52.** H. Wennerström, M. Oliveberg, On the osmotic pressure of cells. *QRB Discovery.* **3,** e12 (2022).

**53.** R. Milo, R. Phillips, N. Orme, "*Cell Biology By the Numbers.*" (Garland Science, New York, 2016), pp. 70, 92, 93, 96, 106, 130, 198.

**54.** M. A. Model, E. Schonbrun, Optical determination of intracellular water in apoptotic cells. *J. Physiol.* **591.23,** 5843-5849 (2013). [DOI: 10.1113/jphysiol.2013.263228]

**55.** W. D. Rooney, G. Johnson, X. Li, E. R. Cohen, S-G. Kim, K. Ugurbil, C. S. Springer, Magnetic field and tissue dependencies of human brain longitudinal $^1H_2O$ relaxation *in vivo*. *Magn. Res. Med.* **57,** 308-318 (2007).

**56.** R. P. Rand, Probing the role of water in protein conformation and function. *Phil. Trans. R. Soc. Lond. B* **359,** 1277-1285 (2004). [DOI 10.1098/rstb.2004.1504]

**57.** P. Ball, Water is an active matrix of life for cell and molecular biology. *Proc. Nat. Acad. Sci.* **114:** 13327-13335 (2017). [doi/10.1073/pnas.1703781114]

**58.** M. Chaplin, Do we underestimate the importance of water in biology. *Nat. Rev. Mol. Cell Biol.* **7,** 862-866 (2006).

**59.** K. D. Garlid, The state of water in biological systems. *Int. Rev. Cytology* **192,** 281-302 (2000).

**60.** F. Persson, B. Halle, Transient access to the protein interior: Simulation versus NMR. *J. Am. Chem. Soc.* **135,** 8735-8748 (2013). [doi.org/10.1021/ja403405d]

**61.** X. L. Lu, V. C. Mow, Biomechanics of articular cartilage and determination of material properties. *Med. Sci. Sports Exerc.* **40,** 193-199 (2008).

**62.** E. Nimer, R. Schneiderman, A. Maroudas, Diffusion and partition of solutes in cartilage under static load. *Biophys. Chem.* **106,** 125-146 (2003). [doi:10.1016/S0301-4622(03)00157-1]

**63.** K. S. Pitzer, in "*Activity Coefficients in Electrolyte Solutions*" (CRC Press, Boca Raton, ed. 2, 1991).

**64.** J. Gao, X. Sun, L. C. Moore, T. W. White, P. R. Brink, R. T. Mathias, Lens intracellular pressure is generated by the circulation of sodium and modulated by gap junction coupling. *J. Gen. Physiol.* **137,** 507 520 (2011).

**65.** R. J. Petrie, H. Koo, Direct measurement of intracellular pressure. *Curr. Protoc. Cell Biol.* **63,** 12.9.1-12.9.9 (2015).

bioRxiv preprint doi: https://doi.org/10.1101/2024.04.17.589812; this version posted April 26, 2024. The copyright holder for this preprint (which was not certified by peer review) is the author/funder, who has granted bioRxiv a license to display the preprint in perpetuity. It is made available under aCC-BY-NC-ND 4.0 International license.




**66.** J. Gao, X. Sun, T. W. White, N. A, Delamere, R. T. Mathias, Feedback regulation of intracellular hydrostatic pressure in surface cells of the lens. *Biophys. J.* **109,** 1830-1839 (2015).

**67.** E. LoCastro, R. Paudyal, Y. Mazaheri, V. Hatzoglou, J. H. Oh, Y. Lu, A. S. Konar, K. vom Eigen, A. Ho, J. R. Ewing, N. Lee, J. O. Deasy, A. Shukla-Dave, Computational modeling of interstitial fluid pressure and velocity in head and neck cancer based on dynamic contrast-enhanced magnetic resonance imaging: Feasibility analysis. *Tomog.* **6,** 129-138 (2020).

**68.** M. DiNuzzo, G. A. Dienel, K. L. Behar, O. A. Petroff, H. Benveniste, F. Hyder, F. Giove, S. Michaeli, S. Mangia, S. Herculano-Houzel, D. L. Rothman, Neurovascular coupling is optimized to compensate for the increase in proton production from nonoxidative glycolysis and glycogenolysis during brain activation and maintain homeostasis of pH, $pCO_2$, and $pO_2$. J. Neurochem. **00,** 1-31 (2023). [DOI:10.1111/jnc.15839]

**69.** H. H. Chowdhury, Differences in cytosolic glucose dynamics in astrocytes and adipocytes measured by FRET-based nanosensors. *Biophys. Chem.* **261,** 106377 (2020).

**70.** I. Schomburg, A. Chang, S. Placzek, C. Sohnigen, M. Rother, M. Lang, C. Munaretto, S. Ulas, M. Stelzer, A. Grote, M. Scheer, D. Schomberg, BRENDA in 2013: Integrated reactions, kinetic data, enzyme function data, improved disease classification: New options and content in BRENDA. *Nucleic Acids Res.* **41,** D764-D772 (2013).

**71.** D. K. Patneau, M. L. Mayer, Structure-activity relationships for amino acid transmitter candidates acting at N-Methyl-D-aspartate and quisqualate Receptors. *J. Neurosci.* **10,** 2385-2399 (1990).

**72.** P. Bisignano, C. Ghezzi, H. Jo, N. F. Polizzi, T. Athoff, C. Kalyanaraman, R. Friemann, M. P. Jacobson, E. M. Wright, M. Grabe, Inhibitor binding mode and allosteric regulation of $Na^+$-glucose symporters. *Nature Comm.* **9,** 5245 (2018).

**73.** J. Jurcovicova, Glucose transport in brain – Effect of inflammation. *Endo. Reg.* **48,** 35-48 (2014). [doi:10.4149/endo_2014_01_35]

**74.** J-H. Lee, R. Liu, J. Li, Y. Wang, L. Tan, X-J. Li, X. Qian, C. Zhang, Y. Xia, D. Xu, W. Guo, Z. Ding, L. Du, Y. Zheng, Q. Chen, P. L. Lorenzi, G. B. Mills, T. Jiang, Z. Lu, EGFR-phosphorylated platelet isoform of phosphofructokinase 1 promotes PI3K activation. *Mol. Cell* **70,** 197-210 (2018).

**75.** X. Xu, A. A. Sehgal, N. N. Yadav, J. Laterra, L. Blair, J. Blakeley, A. Seidemo, J. M. Coughlin, M. G. Pomper, L. Knutsson, P. C. M. van Zijl, D-glucose weighted chemical exchange saturation transfer (glucoCEST)-based dynamic glucose enhanced (DGE) MRI at 3T: Early experience in healthy volunteers and brain tumor patients. *Magn. Reson. Med.* **84,** 247-262 (2020).

**76.** F. A. Nasrallah, G. Pagès, P. W. Kuchel, X. Golay, K-H. Chaung, Imaging brain deoxyglucose uptake and metabolism by GlucoCEST MRI. *J. Cerebr. Blood Flow & Metabol.* **33,** 1270-1278 (2013).

**77.** A. J. Smith, B-J. Jin, A. S. Verkman, Muddying the water in brain edema? *Trends Neurosci.* **38,** 331-332 (2015).

**78.** T. N. Seyfried, L. Shelton, G. Arismendi-Morillo, M. Kalamian, A. Elsakka, J. Maroon, P. Mukherjee, Provocative question: Should ketogenic metabolic therapy become the standard of care for glioblastoma? *Neurochem. Res.* **44,** 2392-2404 (2019).

**79.** K. Nath, D. S. Nelson, D. F. Heitjan, R. Zhou. D. B. Leeper, J. D. Glickson, Effects of hyperglycemia on lonidamine-induced acidification and de-energization of human melanoma xenografts and sensitization to melphalan. (2015). *NMR Biomed.* **28,** 395-403. [DOI:10.1002/nbm.3260]

**80.** H. B. Callen, "Thermodynamics and an introduction to thermostatistics." (Wiley, New York, ed. 2, 1985).

**81.** Y. Jia, S. Xu, G. Han, B. Wang, Z. Wang, C. Lan, P. Zhao, M. Gao, Y. Zhang, W. Jiang, B. Qiu, R. Liu, Y-C. Hsu, Y. Sun, C. Liu, Y. Liu, R. Bai, Transmembrane water-efflux rate measured by magnetic resonance imaging as a biomarker of the expression of aquaporin-4 in gliomas. *Nat. Biomed. Eng.* **7,** 236-252 (2023).[doi.org/10.1038/s41551-022-00960-9]

**82.** C. Tanford, "Physical Chemistry of Macromolecules." (Wiley, New York, 1961).

**83.** H. R. Naito, R. Okamoto, T. Sumi, K. Koga, Osmotic second virial coefficients for hydrophobic interactions as a function of solute size. *J. Chem. Phys.* **156,** 221104 (2022).

bioRxiv preprint doi: https://doi.org/10.1101/2024.04.17.589812; this version posted April 26, 2024. The copyright holder for this preprint (which was not certified by peer review) is the author/funder, who has granted bioRxiv a license to display the preprint in perpetuity. It is made available under aCC-BY-NC-ND 4.0 International license.




**84.** N. A. Perez-Gonzalez, N. D. Rochman, K. Yao, J. Tao, M-T. T. Le, S. Flanary, L. Sablich, B. Toler, E. Crentsil, F. Takaesu, B. Lambrus, J. Huang, V. Fu, P. Chengappa, T. M. Jones, A. J. Holland, S. An, D. Wirtz, R. J. Petrie, K-L. Guan, S. X. Sun, YAP and TAZ Regulate Cell Volume. *J. Cell Biol.* **218,** 3472-3488 (2019).

**85.** K. Sao, T. M. Jones, A. D. Doyle, D. Maity, G. Schevzov, Y. Chen, P. W. Gunning, R. J. Petrie, Myosin II governs intracellular pressure and traction by distinct tropomyosin-dependent mechanisms. *Mol. Biol. Cell* **30,** 1170-1181 (2019).

**86.** M. Shahidullah, A. Mandal, R. T. Mathias, J. Gao, D. Križaj, S. Redmon, N. A. Delamere, TRPV1 activation stimulates NKCC1 and increases hydrostatic pressure in the mouse lens. *Am. J. Physiol. Cell Physiol.* **318,** C969-C980 (2020).

**87.** M. Pallotto, P. V. Watkins, B. Fubara, J. H. Singer, K. L. Briggman, Extracellular space preservation aids the connectomic analysis of neural circuits. *eLife* **4,** e08206 (2015).

**88.** E. A. Neuwelt, Mechanisms of disease: The blood-brain barrier. *Neurosurgery* **54,** 131-142 (2004).

**89.** R. Bai, C. S. Springer, D. Plenz, P. J. Basser, Fast, $Na^+/K^+$ pump driven, steady-state transcytolemmal water exchange in neuronal tissue: A study of rat brain cortical cultures. *Magn. Reson. Med.* **79,** 3207-3217 (2018). [DOI:10.1002/mrm.26980]

**90.** R. Meli, C. Pirozzi, A. Pelagalli, New perspectives on the potential role of aquaporins (AQPs) in the physiology of inflamation. *Front. Physiol.* **9,** 101 (2018).

**91.** L. S. King, D. Kozono, P. Agre. From structure to disease: The evolving tale of aquaporin biology. *Nat. Rev. Mol. Cell Biol.* **5,** 687-698 (2004).

**92.** B. Yang, A. S. Verkman, Water and glycerol permeabilities of aquaporins 1-5 and MIP determined quantitatively by expression of epitope-tagged constructs in Xenopus oocytes. *J. Biol. Chem.* **272,** 16140-16146 (1997).

**93.** L. Hertz, The glutamate-glutamine (GABA) cycle: Importance of late postnatal development and potential reciprocal interactions between biosynthesis and degration. *Front. Endochrinol.* **4,** 59 (2013).

**94.** G. W. Koch, E. Schwartz, Isotopic labeling of metabolic water with $^{18}O_2$. *Rapid Comm. Mass Spectrom.* **37,** e9447 (2023).

**95.** Q. Kuang, P. Purhonen, H. Hebert, Structure of potassium channels. *Cell. Mol. Life Sci.* **72,** 3677-3693 (2015).

**96.** R. P. Rand, V. A. Parsegian, D. C. Rau, Intracellular osmotic action. *Cell. Mol. Life Sci.* **57,** 1018-1032 (2000).

**97.** H. Wiebe, J. Spooner, N. Boon, E. Deglint, E. Edwards, P. Dance, N. and Weinberg, Calculation of molecular volumes and volumes of activation using molecular dynamics simulations. *J. Phys. Chem. C* **116,** 2240-2245 (2012). [doi.org/10.1021/jp209088u]

**98.** C. D. Hubbard, R. van Eldik, Mechanistic information on some inorganic and bioinorganic reactions from volume profile analysis. *Inorg. Chim. Acta* **363,** 2357-2374 (2010). [doi: 10.1016/j.ica.2009.09.042]

**99.** A. Drljaca, C. D. Hubbard, R. van Eldik, T. Asano, M. V. Basilevsky, W. J. le Noble, Activation and reaction volumes in solution. 3. *Chem. Revs.* **98,** 2167-2289 (1998).

bioRxiv preprint doi: https://doi.org/10.1101/2024.04.17.589812; this version posted April 26, 2024. The copyright holder for this preprint (which was not certified by peer review) is the author/funder, who has granted bioRxiv a license to display the preprint in perpetuity. It is made available under aCC-BY-NC-ND 4.0 International license.



## *Appendix A.1. Acronyms and Symbols.*

⟨A⟩ tissue or voxel mean cell surface area
AQP aquaporin
AQP4 aquaporin 4
AQP4KO aquaporin 4 knock-out
ATP adenosine triphosphate
$ATP_i$ intracellular ATP
AWC active trans-membrane water cycling
$a_e$ $\rho\langle A\rangle$
$a_{H2O}$ water thermodynamic activity
CEST chemical exchange saturation transfer
ΔG Gibbs free energy change
$\Delta G^0$ Standard ΔG
$\Delta G_{YYY}$ ΔG for substrate, enzyme, reaction; YYY
$\Delta G_{YYY}$(effl) ΔG for YYY efflux
$\Delta G_{YYY}$(infl) ΔG for YYY influx
$\Delta H_{YYY}$(infl) enthalpy change for YYY influx
$\Delta\pi_{oi}$ trans-cytolemmal osmotic gradient (in – out)
$\Delta S_{YYY}$(infl) entropy change for YYY influx
$\Delta V^{\dagger\dagger}$ activation volume
d density (mass/volume)
EAAT1 excitatory amino acid transporter 1
$E_{m,oi}$ trans-membrane electrical potential (in – out)
effl an efflux process
FDG 2-deoxy-2-$^{18}$Fluoro-D-glucose
$f_{H2O}$ water activity coefficient on the mole fraction scale (X)
$f_W$ tissue water volume fraction
$f_{W,i}$ intracellular $f_W$
$f_{W,o}$ extracellular $f_W$
$\phi$ osmotic coefficient
G Gibbs free energy
GABA γ-amino butyric acid
GAT1 GABA transporter 1
GLUT1 glucose transporter 1
glc glucose
gln glutamine
glu glutamate$^-$
$\gamma_{H2O}$ water activity coefficient on the molality scale (m)
$^1H_2O$ water proton MR signal
$H_2O_i$ intracellular water molecule
$H_2O_o$ extracellular water molecule
$H_3O_i^+$ intracellular hydronium ion
$H_3O_o^+$ extracellular hydronium ion
iGlutR an ionotropic glutamate$^-$receptor
infl an influx process
$K_i^+$ intracellular $K^+$
$K_o^+$ extracellular $K^+$
KCC4 potassium, chloride transporter 4
k kinetic rate constant
$k_{io}$ cellular water efflux k ($1/\tau_i$)
$k_{io}$(a) active $k_{io}$ contribution
$k_{io}$(p) passive $k_{io}$ contribution
$k_{oi}$(p) passive cellular water influx k contribution
M molarity concentration scale
MADI metabolic activity diffusion imaging
MCT1 mono-carboxylate transporter
MD molecular dynamics
MRI magnetic resonance imaging
$MR_{YYY}$ YYY metabolic rate
$MR_{glu}$(consump) MR of glucose consumption
$MR_{glu}$(infl) MR of glucose influx
$MR_{Glu\text{-}gln}$(cycle) MR of glutamate$^-$-glutamine cycling
$MR_{O2}$ MR of O2 consumption
$^cMR_{YYY}$ cellular metabolic rate for YYY process = $^tMR_{YYY}/\rho$
$^tMR_{YYY}$ tissue metabolic rate for YYY process = $\rho{}^cMR_{YYY}$
$MW_{H2O}$ molecular mass ("weight") of water
m molality concentration scale
mOsM milli-osmolarity concentration scale
mOsm milli-osmolality concentration scale
mOsX milli-osmole fraction concentration scale
$\mu_{YYY}$ chemical potential of YYY; $(\partial G/\partial n_{YYY})_{T,P,n(\neq nYYY)}$
$Na_i^+$ intracellular $Na^+$
$Na_o^+$ extracellular $Na^+$
NKA $Na^+$,$K^+$-ATPase (sodium pump)
NKCC1 sodium, potassium, chloride transporter 1
NMR nuclear magnetic resonance
n number of moles
OsM osmolarity concentration scale
$OsM_{YYY}$ YYY OsM
Osm osmolality concentration scale
$Osm_{YYY}$ YYY Osm
OsX osmole fraction concentration scale
$OsX_{YYY,i}$ intracellular YYY OsX
$OsX_{YYY,o}$ extracellular YYY OsX
P hydraulic (mechanical) pressure
$P^0$ standard state P
$P_d$ diffusional permeability coefficient (exchange)
$P_d$(p) passive $P_d$
$P_{dYYY}$ YYY $P_d$
$P_f$ flux (flow) permeability coefficient
$P_{fYYY}$ YYY Pf
$P_i$ intracellular P
$P_o$ extracellular P
PC potassium channel
PET positron emission tomography
p tissue water mole fraction ("population")
$p_i$ intracellular p
$p_o$ extracellular p
per permeant particle
R ideal gas constant
**ρ** cell (number) density
$S_{YYY}$ stoichiometric coefficient of YYY
SGLT sodium/glucose co-transporter
SS trans-cytolemmal NMR shutter-speed
TGN020 specific AQP4 inhibitor
$\tau_i$ mean $H_2O_i$ molecule lifetime ($1/k_{io}$)
⟨V⟩ tissue or voxel mean cell volume
$_Vm$ volume molality concentration scale
$_Vm_i$ intracellular $_Vm$
$_Vm_o$ extracellular $_Vm$
v tissue volume fraction
$v_e$ extracellular v (ECV) (= $1 - v_i$)
$v_i$ intracellular v [**ρ**V]
X mole fraction concentration scale
$X_{YYY}$ YYY X
$X_{YYY,i}$ intracellular YYY X
$X_{YYY,o}$ extracellular YYY X
x water cycling stoichiometry [$H_2O$/ATP]
x′ x for individual water co-transporter
[YYY] YYY concentration
$[YYY_c]$ compartmental YYY concentration
$[YYY_i]$ intracellular YYY concentration
$[YYY_o]$ extracellular YYY concentration
$[YYY_t]$ tissue YYY concentration = $v_i[YYY_i] = v_e[YYY_o]$
yL yocto liter (= $10^{-24}$ L = 1 $(nm)^3$))
$y_{H2O}$ water activity coefficient on the molarity scale (M)
$Z_{YYY}$ signed electrical charge of YYY

bioRxiv preprint doi: https://doi.org/10.1101/2024.04.17.589812; this version posted April 26, 2024. The copyright holder for this preprint (which was not certified by peer review) is the author/funder, who has granted bioRxiv a license to display the preprint in perpetuity. It is made available under aCC-BY-NC-ND 4.0 International license.



**A.2. Compartmental Water Thermodynamic Activities.**

Solvent mole fraction values as large as $OsX_{H2O,o}$ = 0.995 and $OsX_{H2O,i}$ = 0.993 (Table 1) "fail to emphasize the departure from ideality indicated by the activity coefficient of the *solute*" ((45), p.29). However, here the *solvent* activity coefficient difference is also very small. Since the water activity $a_{H2O}$ (dimensionless on this scale) is always so close to unity, it requires sophisticated apparatus for high-precision direct water vapor pressure determinations to measure (45). Using these, it has been found $a_{H2O}$ is inversely, and exponentially, related to the solute osmolality, $Osm_{solute}$, *via* the empirical *osmotic coefficient*, $\varphi$, **Equation (A.2.1)** (19,45,46; (63), p.12). $MW_{H2O}$ is the water molecular

$$a_{H2O} = e^{-\left(\varphi \bullet MW_{H2O} \bullet Osm_{solute}/1000\right)} = e^{-(\varphi \bullet 0.018054 \bullet Osm_{solute})} \qquad \text{(A.2.1)}$$

weight (mass), 18.0154 g/mole($H_2O$). The dimensionless product ($MW_{H2O}$•$Osm_{solute}$/1000) is the solute/solvent mole ratio (1000 is (g/kg)), and essentially the solute mole fraction, $OsX_{solute}$. The latter is also dimensionless, and since the exponent must be dimensionless, $\varphi$ is also dimensionless. Equation (A.2.1) provides a way to evaluate $a_{H2O}$. (When $Osm_{solute}$ is zero (pure water), $a_{H2O}$ is exactly one.)

How might we more fruitfully evaluate Eq. (4) when per = $H_2O$? Solutions as complex as those in Table 1 have never been subjected to precise measurements such as those of the last paragraph. However, pure NaCl and KCl solutions have been so studied, at 298 K ((45), p.476). We could take as a surrogate interstitium 0.290 Osm NaCl, and a surrogate cytosol 0.375 Osm KCl. (A glance at the metabolomics study mentioned above (47) indicates a $K^+$glutamate$^-$ solution would be a better intracellular surrogate. However, that has never been studied.) Their respective osmotic coefficients are $\varphi_o$ = 0.9249 and $\varphi_i$ = 0.9141 ((45), p.476) and, *via* Eq. (A.2.1), give $a_{H2O,o}$ = 0.995 and $a_{H2O,i}$ = 0.994. Using these activities in Eq. (4) gives $\Delta$G(infl) = - 0.003 kJ/mole for $H_2O$ influx. This free energy change is again so small that correcting for temperature and actual solute content would make no difference. The conclusion is inescapable: there is a very small trans-membrane chemical potential difference (~3 J/mole) for water to enter the cell.

bioRxiv preprint doi: https://doi.org/10.1101/2024.04.17.589812; this version posted April 26, 2024. The copyright holder for this preprint (which was not certified by peer review) is the author/funder, who has granted bioRxiv a license to display the preprint in perpetuity. It is made available under aCC-BY-NC-ND 4.0 International license.



**A.3. Intracellular Pressure and Kinetics (Reaction Activation Volumes).**

Mechanical pressure can affect transporter free energies (as above), and macromolecular structures (96), but can also exert an effect on chemical reaction kinetics. This is characterized by the volume of activation, $\Delta V^{\dagger\dagger}$, the difference between the partial molar volume of the reaction transition state and the partial molar volume of the reactants (97-99). The pressure dependence of a rate constant, k, is expressed in **Equations (A.3.1) and (A.3.2)**,

$$\frac{\partial lnk}{\partial P} = -\frac{\Delta V^{\dagger\dagger}}{RT} = -\frac{\Delta V^{\dagger\dagger}}{25.4} \qquad \text{(A.3.1)}$$

$$\frac{k_A}{k_B} = e^{\left[\left(\Delta V^{\dagger\dagger}/_{RT}\right)(P_B - P_A)\right]} \qquad \text{(A.3.2)}$$

where RT is 25.4 L•atm/mole at 310 K. If a process has $\Delta V^{\dagger\dagger}$ = 6 L/mole, a 10 atm pressure increase will cause its rate constant to decrease by 90%. Six L/mole is $10^{-23}$ L/molecule, or 10 yL/molecule (1 yocto liter = 1 yL = $10^{-24}$ L = 1 $(nm)^3$). The plasma membrane NKA is a macromolecular complex of mass 145 kDa (145,000 g/mole). Thus (assuming d = 1 g/mL), it has a partial molar volume of approximately 242 yL/molecule. A 6 yL $\Delta V^{\dagger\dagger}$ would represent only a 2.5 % volume change. For $P_i$ = 1.5 atm (the maximum $P_i$ reported), $P_o$ = 1 atm, and $\Delta V^{\dagger\dagger}$ = 6 L/mole, Eq. (A.3.2) yields $k_{1.5\ atm} = 0.89\ k_{1\ atm}$, an 11% decrease.

It is easy to imagine $\Delta V^{\dagger\dagger}$ values of this magnitude, or greater. In a molecular dynamics study of a small 6.5 kDa protein, Persson and Halle report a relatively constrained, 2 kDa domain undergoes numerous spontaneous 3% conformational volume fluctuations in a 1000 μs period (60). Most membrane transporters are rather large macromolecular complexes. It is quite likely they undergo significant absolute volume changes in reaching their transition states. Thus, their enzyme activities could be quite sensitive to intracellular pressure development. Some would slow down, and some would speed up: $\Delta V^{\dagger\dagger}$ quantities can be negative (97-99). Furthermore, the activities of most membrane transporters are coupled to each other *via* common substrates or products (Fig. 1). Since the cell has evolved to have trans-membrane fluxes in homeostatic balance, it is likely a $P_i$ change would disturb the latter. The consequent flux changes could serve an auto-regulatory function.